Chapter 4

GluClv2.0: An Improved Tool For Neuronal Silencing

Abstract

A variety of genetically encoded tools have been developed that allow physical manipulation of neuronal excitability in a reversible, cell-specific manner. We previously engineered an invertebrate glutamate-gated chloride channel (GluCl αβ) that enabled pharmacologically induced silencing of electrical activity in targeted CNS neurons *in vivo* by the anthelmintic drug compound ivermectin (IVM). With this receptor, GluCl opt α-CFP + opt β-YFP Y182F, the concentration of IVM necessary to elicit a consistent silencing phenotype was high enough to raise concern about its potential side effects. Variability in the extent of spike suppression was also apparent and correlated with co-expression levels of the fluorescently tagged α and β subunits. To address these issues, mutant receptors were generated via rational protein engineering strategies and subjected to functional screening and fluorescence-based assays. It has since been learned that GluCl α homomers are indeed expressed at the plasma membrane and are responsive to IVM, but incorporation of the β subunit confers greater IVM sensitivity. Introduction of a gain-of-function mutation (L9'F) in the second transmembrane domain of the α subunit appears to facilitate β subunit incorporation and substantially increase heteromeric GluCl αβ sensitivity to IVM without permitting unliganded channel opening. Removal of an arginine-based ER retention motif (RSR mutated to AAA) from the intracellular loop of the β subunit further promotes heteromeric expression at the plasma membrane by preventing ER-associated degradation of the β subunit. Introduction of a monomeric XFP mutation (A206K) complements these effects. The newly engineered GluCl opt α-mXFP L9'F + opt β-mXFP Y182F RSR_AAA receptor significantly increases conductance and

reduces variability in evoked spike generation *in vitro* using a lower concentration of IVM. This receptor, dubbed 'GluClv2.0', is an improved tool for IVM-induced silencing.

Introduction

Neurons are organized into anatomically distinct regions that transmit excitatory or inhibitory information to the regions they project to, following a specific pathway or circuit. Inappropriate activity within such a circuit is thought to be the basis of most psychiatric and neurological disorders. Unraveling the intricate circuitry and functional basis of various neuronal networks will provide a better understanding of complex behavior and help pinpoint the underlying causes of brain related dysfunction.

A number of tools have been developed that allow the physical manipulation of neuronal excitability in a reversible, cell-specific manner. These tools enable mapping of neuronal connectivity and are essential for assigning functional roles to particular cell types and determining their contribution to perception or behavior. One such tool employs a heteromeric glutamate-gated chloride channel (GluCl αβ) from the invertebrate species *Caenorhabditis elegans* and the anthelmintic drug compound ivermectin (IVM). IVM-induced activation of GluCl αβ heterologously expressed in mammalian neurons elicits a chloride conductance that drives the membrane potential toward the Nernst potential of chloride (E_{Cl}) to prevent action potential generation for effective neuronal silencing.

The GluCl/IVM method was the first to show neuronal silencing induced by a systemically administered drug in awake, behaving animals[1]. In this study, proof-of-concept was demonstrated in mice using a robust and reproducible striatal lesion assay known to induce amphetamine-dependent rotational behavior[2,3]. In mice expressing GluCl unilaterally in the striatum via AAV2-mediated infection, systemic administration

of IVM caused unidirectional rotation of the animal, indicating that striatal neurons were silenced (Figure 4-1A). The rotational phenotype was observed within hours of induction and was fully reversed within days, allowing multiple cycles of silencing and recovery to be performed on a single animal.

IVM is a widely used commercial drug that is well tolerated by both animals and humans because GluCl channels do not exist in mammals. Selective and reversible silencing was achieved without measurable toxicity of either the individual neurons or the animal as a whole. However, the dose of IVM required to elicit a consistent silencing phenotype (5–10 mg/kg; Figure 4-1B)[1] was unexpectedly higher than that routinely used to treat mice with parasitic infections (0.2 mg/kg)[4] and high enough to raise concern about potential side effects. Though IVM can successfully cross the BBB, some fraction is presumably being cleared continuously from the brain by the mdr1a P-glycoprotein transporter[5], resulting in a lower effective concentration in the cerebrospinal fluid. Further increasing the dose (20 mg/kg) enters the range of toxicity, visible by paralysis[6]. Toxic effects are likely mediated through off-target agonism, as IVM is known to activate or potentiate other ligand-gated ion channels present in the CNS, though it does so with much lower affinity[7-10].

Silencing experiments with the GluCl/IVM system were also subject to considerable variability. Rotation data from the *in vivo* study displays a bimodal distribution with one group of animals exhibiting a weak but significant phenotype, and the other exhibiting a strong behavioral phenotype. The strength of the behavioral phenotype was correlated with both the extent of viral infection (i.e., the volume of striatum expressing GluCl $\alpha\beta$) and the extent of spike suppression (i.e., individual

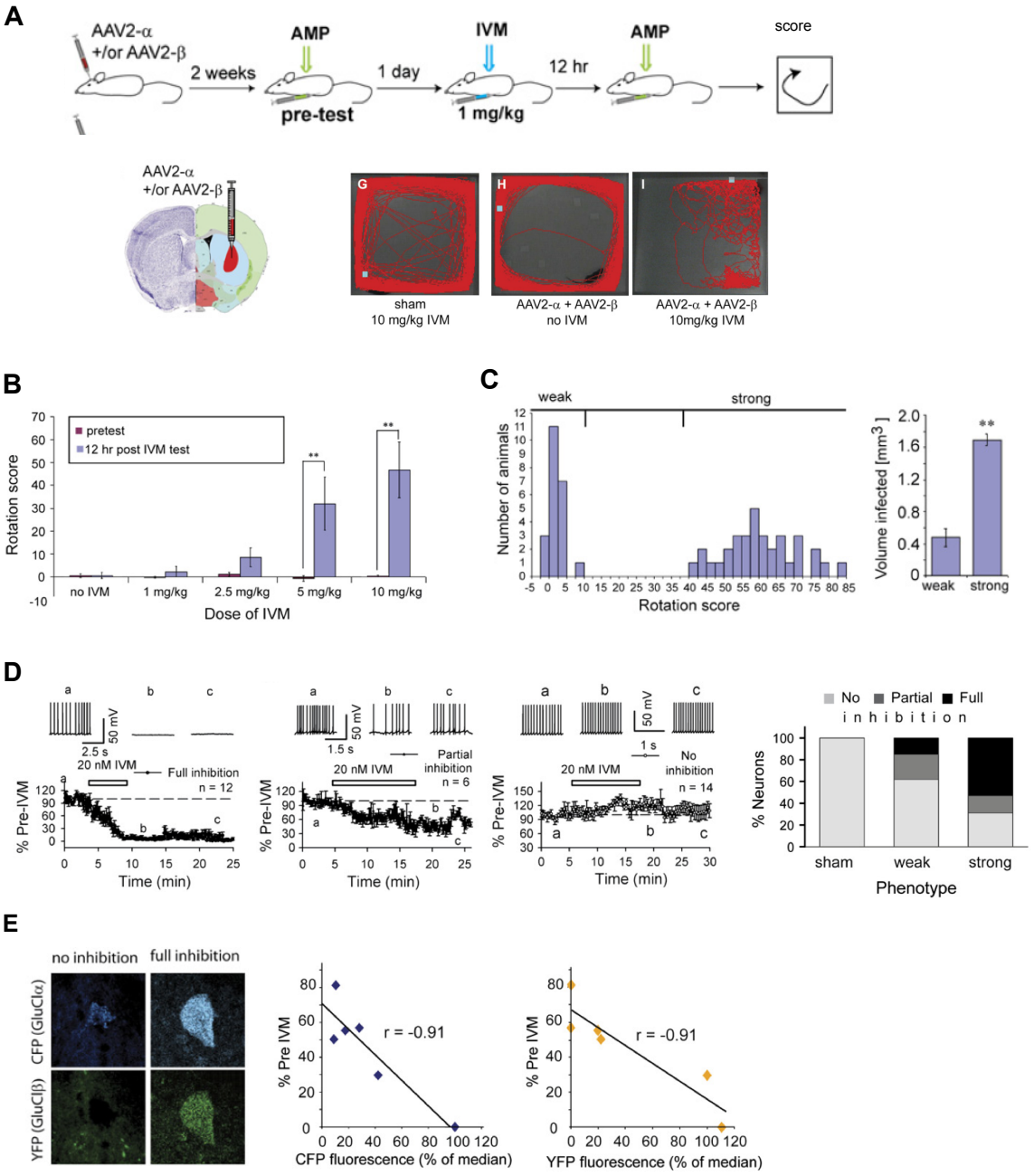

Figure 4-1. Proof-of-concept for GluCl/IVM neuronal silencing *in vivo*. *A*. Experimental design schematic of amphetamine-induced rotation test for silencing striatal neurons. Unilateral striatum was virally infected with GluCl α and β subunits. Control mice move around the chamber perimeter. Mice expressing GluCl and administered IVM display rotational behavior. *B*. Dose-response relation for amphetamine-induced rotation. *C*. Histogram of rotation score shows bimodal distribution. Strength of the phenotype correlates with the volume of the virally infected region. *D*. Neuron firing rates show full, partial and no inhibition. Lowercase letters display sample spike trains before (a) and after (b & c) IVM perfusion. Strength of the phenotype correlates with the extent of spike suppression. *E*. Confocal images show varying subunit expression levels. Extent of spike suppression is correlated with fluorescence intensity of α-CFP and β-YFP Y182F subunits. (Figures adapted from Lerchner et al., 2007.)[1]

neurons showing either full, partial, or no inhibition), which further correlated with co-expression levels of α and β subunits (Figure 4-1C, D, E).

Prior to its implementation as a silencing tool, the GluCl receptor was modified in several ways. First, it was rendered insensitive to its native ligand glutamate by a single point mutation in the β subunit, Y182F (Figure 4-2A)[11]. Insensitivity is necessary since glutamate is an endogenous neurotransmitter present in cerebrospinal fluid and released during synaptic transmission. In addition, the DNA sequence of this invertebrate gene was codon-optimized to achieve greater expression levels in mammalian systems (Figure 4-2B)[12], and tagged with fluorescent proteins YFP and CFP for direct visualization of protein expression (Figure 4-2C)[11]. This GluCl opt α-CFP + opt β-YFP Y182F receptor is referred to throughout this study as 'the original tool'.

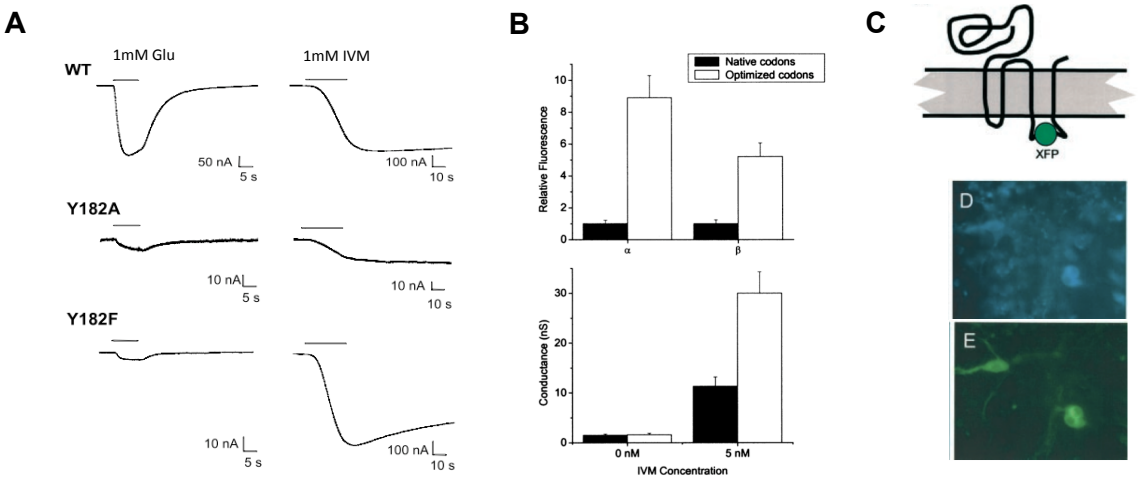

Figure 4-2. Construct modifications generating the original GluCl opt α-CFP + opt β-YFP Y182F silencing tool. *A.* A tyrosine-to-phenylalanine mutation at position 182 of the β subunit abolishes glutamate sensitivity but maintains activation by IVM. *B.* Codon optimization of GluCl subunits increased expression levels in mammalian cells. *C.* Fluorescent labels, CFP and YFP, were inserted into the intracellular M3-M4 loop for direct visualization of subunit expression. (Figures adapted from Li et al., 2002; Slimko et al., 2002; Slimko & Lester, 2003.)[11-13]

The current study aimed to optimize the original GluCl/IVM tool by introducing rational point mutations intended to (1) increase receptor sensitivity to IVM in order to achieve silencing by lower doses and, (2) improve subunit expression at the plasma membrane in order to reduce spike suppression variability. Such optimization would alleviate the concern of off-target side effects and avoid suboptimal spike inhibition. As was the subject of Chapter 3, introduction of an L9'F gain-of-function mutation in the second transmembrane domain of the α subunit appears to facilitate β subunit incorporation and substantially increase heteromeric GluCl αβ sensitivity to IVM without permitting unliganded channel opening. Glutamate insensitivity must be reinstated to this high sensitivity mutant receptor for it to function effectively as a silencing tool. It was also determined that GluCl α homomers are indeed expressed at the plasma membrane of mammalian cells and are responsive to IVM. A mixed presence of heteromeric and homomeric receptors could be responsible for the variability in spike suppression. To address this possibility in the current study, the secretory pathway of membrane receptor trafficking was considered. Rational protein engineering strategies to improve heteromeric GluCl αβ surface expression may be combined with the increased sensitivity mutation to produce an optimized GluCl/IVM silencing tool.

Results

Mutation of a putative ER retention motif enhances IVM sensitivity

In the cell, multimeric receptors destined for the plasma membrane are synthesized, matured, and assembled at the endoplasmic reticulum (ER)[14,15]. The amino acid sequence contains specific signaling motifs that instruct the cellular machinery to either let the protein exit the ER or retain it there. Subunits that have been assembled into complete receptors are prepared for ER export at 'exit sites' where they are packaged into coat protein II (COPII) vesicles that mediate anterograde transport from the ER to the Golgi. In the Golgi, receptors are either subject to posttranslational modifications after which they are trafficked to the plasma membrane, or they undergo retrograde transport (i.e., retrieval) by COPI vesicles back to the ER. This ER retention-retrieval process serves as a quality control mechanism to ensure that only properly assembled receptors are transported to the cell surface. Proteins that are misfolded, unassembled, or improperly assembled are retained in the ER and ultimately targeted for ER-associated degradation[16,17].

Consensus signaling motifs exist for both ER export and ER retention. The best-characterized exit signals include DxE[18,19], LxxL/ME[20], and I/LxM[21]. These ER export motifs are found on the cytosolic loops of a variety of membrane-associated proteins and are recognized by Sec24, the primary cargo-selection protein of the COPII coated vesicles for transport from ER to Golgi. Well-described ER retention signals include the classical C-terminal motifs, KDEL and KKxx[22,23], and the cytosolic arginine-based signal, RxR[24]. The RxR motif has been found in potassium channels[24], G-protein coupled

receptors[25], voltage-dependent Ca^{2+} channels[26], ionotropic glutamate receptors[27-29] and ionotropic Cys-loop receptors[30-32]. Proteins containing an RxR motif are retained in the ER or maintained by COPI retrieval until the signal is masked as a result of heteromultimeric assembly with additional subunits[33-35].

To check for putative ER signaling motifs present in GluCl α and β, the amino acid sequence of the large TM3–TM4 intracellular loop of each subunit was examined (Figure 4-3). The α subunit has one potential ER export motif, LNLLE, immediately following the fluorescent fusion protein insertion (note, XFP tags were originally placed in TM3–TM4 loop at restriction sites[11]). The β subunit has two putative ER export motifs, LEM and DAE, as well as two putative ER retention motifs, RSR and RRR. The presence of these possible signaling motifs correlates with functional expression observed for each of these subunits in mammalian systems. In HEK293 cells, heteromeric GluCl αβ channels are activated by glutamate and IVM; α homomers form functional channels at the plasma membrane responsive to IVM, while no response is observed for β homomers with either glutamate or IVM. It is possible that one or both of the ER retention motifs present in the β subunit prevents its trafficking to the plasma membrane in the absence of α subunits, fitting with the premise that subunits bearing an arginine-based ER retention motif require 'masking' by assembly with other appropriate subunits in order to exit the ER. It also suggests that variability in receptor expression and silencing could be due to ER retention of the β subunit. Thus, removal of ER retention signals may allow more uniform receptor expression and consistent neuronal silencing. To test this hypothesis, the putative ER retention motifs of GluCl β were mutated to

alanine residues: GluCl β-YFP R318A, S319A, R320A for a 'RSR_AAA mutant' and GluCl β-YFP R329A, R330A, R331A for a 'RRR_AAA mutant'.

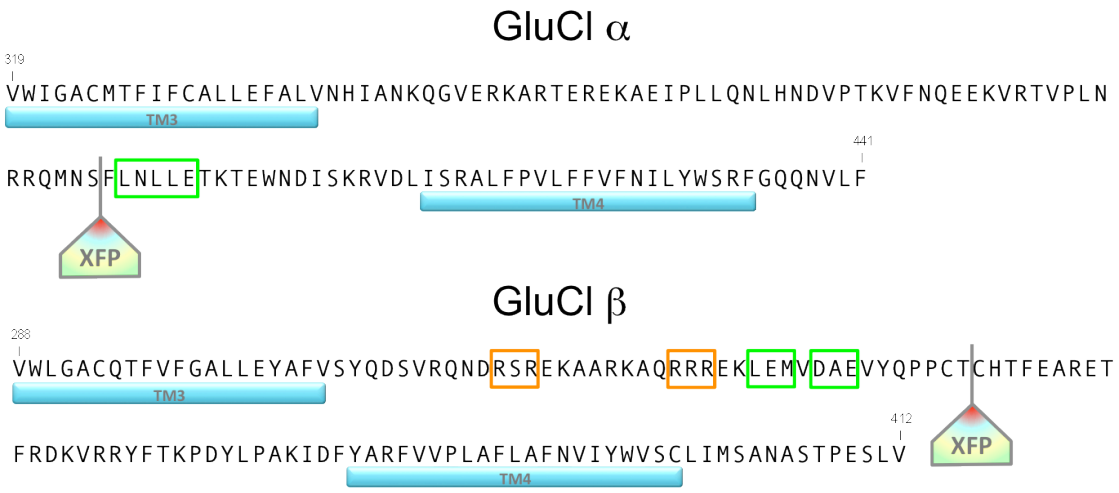

Figure 4-3. Putative ER signaling motifs in GluCl α and β subunits. Amino acid sequence including the intracellular TM3–TM4 loop of GluCl α and GluCl β subunits. The last amino acid of each sequence is the C-terminal residue. Transmembrane spanning helices (TM3 and TM4) are defined by blue rectangles. Position of the fluorescent protein insertion is noted by 'XFP'. ER export motifs are shown in green boxes; ER retention motifs are shown in orange boxes. The α subunit contains a single putative ER export motif (LxxL/ME). The β subunit contains two possible ER export motifs (I/LxM; DxE) and two potential ER retention motifs (RxR).

Mutant β subunits were expressed as heteromeric receptors and tested for IVM activation using a membrane potential assay to ensure that the RSR_AAA and RRR_AAA mutations did not disrupt channel function. The α-YFP + β-YFP RSR_AAA and α-YFP + β-YFP RRR_AAA mutant receptors, and the double mutant receptor, α-YFP + β-YFP RSR_AAA&RRR_AAA, each displayed a concentration-dependent IVM response similar to the WT and WT-XFP receptors (Figure 4-4A, Table 4-1). No

response was observed for any of the mutated β subunits when transfected in the absence of the α subunit, suggesting that removal of these putative retention motifs is not sufficient to allow membrane expression of β homomers. Noticeable differences including a biphasic dependency of the (β)RSR_AAA mutant and increased raw RFU signal (Figure 4-4B) for both the (β)RSR_AAA and (β)RRR_AAA mutants conveyed these mutations were having an effect. Removal of an ER retention motif could either be increasing the total number of receptors expressed at the surface, or shifting the receptor subunit stoichiometry, or both.

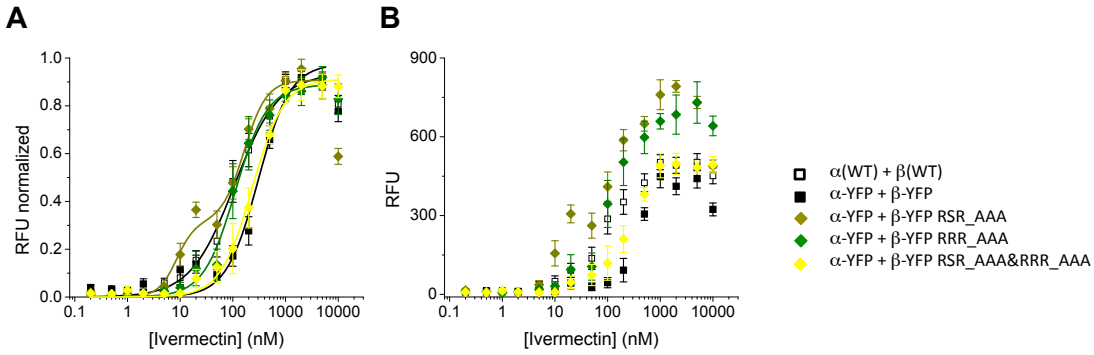

Figure 4-4. Ivermectin concentration-response curves for putative ER retention mutants. IVM activation was assayed using the FlexStation. *A*. Normalized IVM concentration-response curves for the heteromeric (β)RSR_AAA, (β)RRR_AAA, and (β)RSR_AAA&RRR_AAA mutant receptors are similar to WT and WT-XFP. IVM activation parameters are shown in Table 4-1. *B*. The (β)RSR_AAA and (β)RRR_AAA mutants show increased raw RFU signals.

If removal of the putative retention motifs increases the number of receptors trafficked to the plasma membrane, it should result in greater whole-cell currents. Avoiding the issues with IVM electrophysiology as discussed in the previous chapter, glutamate-induced currents of the heteromeric (β)RSR_AAA and (β)RRR_AAA mutant receptors were recorded in whole-cell patch-clamp mode using the Dynaflow microperfusion chip. Pooled concentration-response relations of these mutants were again similar to WT and WT-XFP, but there was no statistically significant increase in maximal current for the number of cells recorded (Figure 4-5A, B). Multiple sensitivities were observed as before (Figure 4-5C; Chapter 3, Figure 3-3) with comparable EC_{50} values and a greater number of cells showing a 'low sensitivity' response to glutamate.

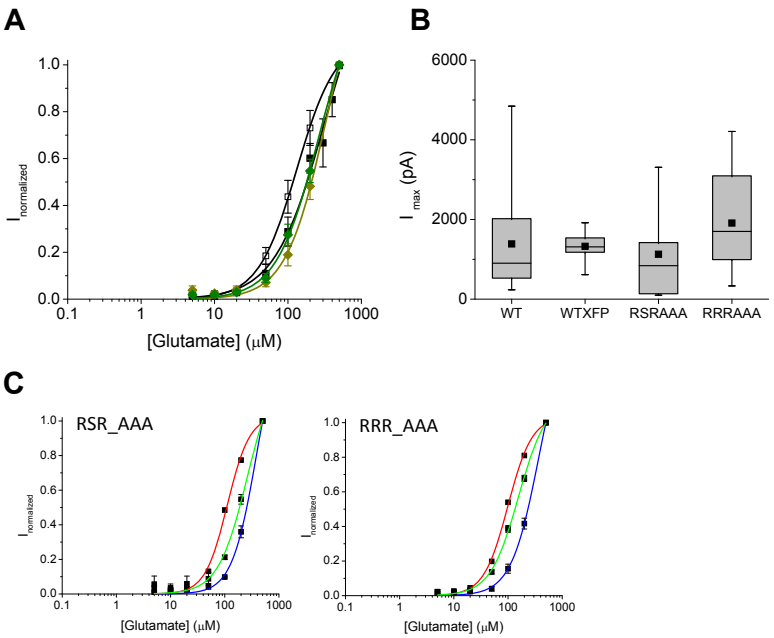

GluCl channel	abbr.	EC_{50} (μM)	Hill	n
α(WT) + β(WT)	WT	314 ± 133*	1.28 ± 0.23	14
α-YFP + β-CFP	WT-XFP	132 ± 5	1.64 ± 0.07	12
α-YFP + β-YFP RSR_AAA	RSR_AAA	331 ± 88	1.57 ± 0.22	8
α-YFP + β-YFP RRR_AAA	RRR_AAA	262 ± 30	1.50 ± 0.11	11

	High Sensitivity			Mixed			Low Sensitivity		
	EC_{50} (μM)	Hill	n	EC_{50} (μM)	Hill	n	EC_{50} (μM)	Hill	n
WT	44.71 ± 0.00	3.05 ± 0.17	1	159.65 ± 0.01	2.03 ± 0.12	9	2564.9 ± 3.98*	1.45 ± 0.15	4
WT-XFP	80.68 ± 0.00	2.22 ± 0.13	6	145.91 ± 0.02	1.49 ± 0.16	3	306.90 ± 0.01*	2.41 ± 0.09	3
RSR_AAA	111.90 ± 6.79	2.11 ± 0.21	1	262.22 ± 78.65	1.61 ± 0.33	3	385.27 ± 123.6	1.92 ± 0.35	4
RRR_AAA	99.56 ± 4.70	1.95 ± 0.14	1	155.62 ± 8.56	1.67 ± 0.09	4	368.23 ± 79.14	1.71 ± 0.19	6

Figure 4-5. Glutamate concentration-response curves for putative ER retention mutants. Glutamate activation was assayed by whole-cell electrophysiology. *A*. Normalized glutamate concentration-response curves for heteromeric (β)RSR_AAA and (β)RRR_AAA mutant receptors are similar to WT and WT-XFP. *B.* Maximal glutamate-induced currents of the mutant receptors are not significantly different from WT and WT-XFP. *C.* Concentration response curves of individual cells could be separated into three categories: high sensitivity (red line), low sensitivity (blue line), and mixed (green line). Glutamate activation parameters for putative ER retention mutants are presented in the corresponding tables. Curves for cell-to-cell variability of WT and WT-XFP are shown in Chapter 3, Figure 3-3. The EC_{50} and Hill coefficient values represent the mean ± SEM for the number of cells (n) recorded. The * indicates concentration-response normalization to a less-than-saturating maximum concentration.

In the previous chapter, introduction of an (α)L9'F mutation yielded a biphasic concentration-dependent relationship with increased sensitivity to IVM (Chapter 3, Figure 3-6). Addition of the (α)L9'F mutation with the putative ER retention mutations produced pronounced two-component relationships for both the (α)L9'F + (β)RSR_AAA and the (α)L9'F + (β)RSR_AAA&RRR_AAA mutant receptors (Figure 4-6A). In particular, the (α)L9'F + (β)RSR_AAA mutant receptor shows a significant increase in activation with low (10 nM) concentrations of IVM (Figure 4-6B).

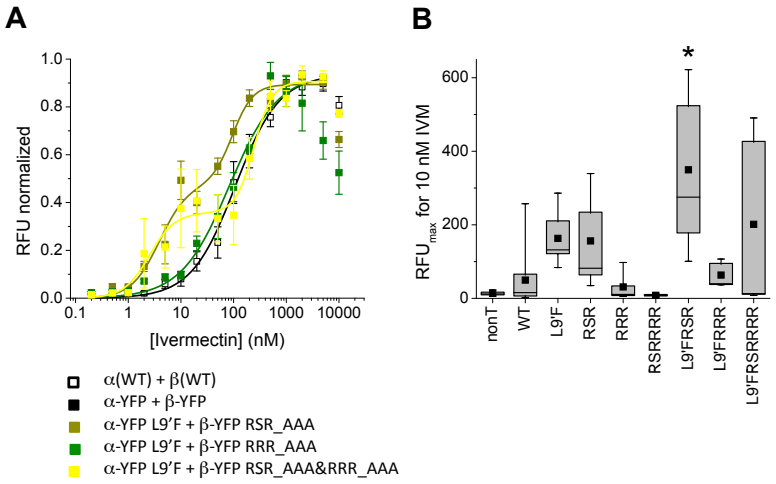

Figure 4-6. IVM concentration-response curves for putative ER retention mutants plus the (α)L9'F mutation. IVM activation was assayed using the FlexStation. *A*. Normalized IVM concentration-response curves for (α)L9'F + (β)RSR_AAA and (α)L9'F + (β)RSR_AAA&RRR_AAA show a pronounced biphasic relationship. IVM activation parameters are shown in Table 4-1. *B*. The (α)L9'F + (β)RSR_AAA mutant receptor is significantly more sensitive to 10 nM IVM than WT.

Glutamate insensitive mutations eliminate increased sensitivity to IVM

The significant increase in IVM sensitivity was encouraging toward the goal of GluCl optimization. The (α)L9'F and β subunit ER retention mutations tested up to this point, however, had been examined using glutamate-sensitive receptors. True optimization of the silencing tool requires glutamate insensitivity, accomplished by the binding site mutation, Y182F, in the β subunit. Astonishingly, reintroduction of the (β)Y182F mutation into the (α)L9'F + (β)RSR_AAA receptor abolished the high IVM sensitivity component of the biphasic concentration-response curve (Figure 4-7A). The same loss of high IVM sensitivity was observed when the glutamate insensitive (β)Y182F mutation was restored to the individual (α)L9'F and (β)RSR_AAA mutant receptors (Figure 4-7B, C).

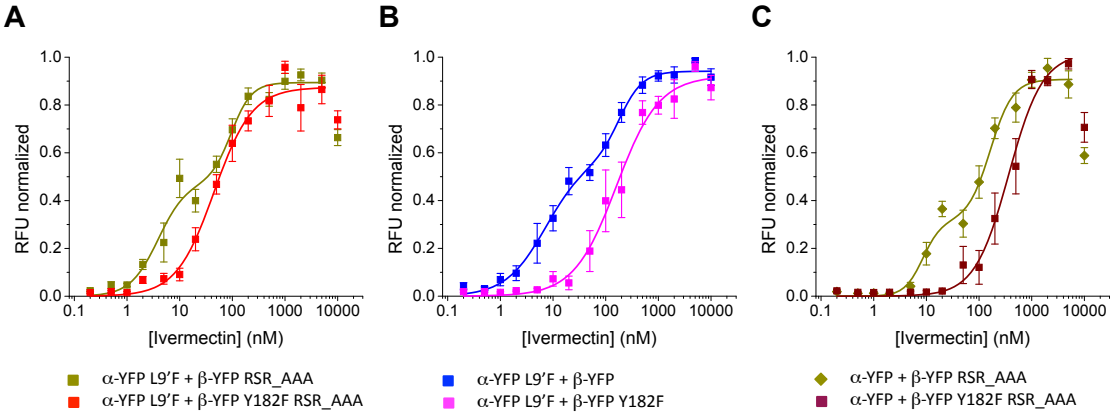

Figure 4-7. Reintroduction of a glutamate insensitive mutation affects IVM sensitivity of proposed optimized receptor. IVM activation was assayed using the FlexStation. Normalized IVM concentration-response curves show presence of a (β)Y182F mutation eliminates the high sensitivity component of the biphasic relationship for the combined (α)L9'F + (β)RSR_AAA mutant receptor (*A)* as well as the individual (α)L9'F and (β)RSR_AAA mutant receptors (*B&C*). IVM activation parameters are shown in Table 4-1.

In spite of these effects, the (β)Y182F mutation alone was confirmed to behave as expected, rendering heteromeric GluCl αβ receptors insensitive to glutamate without affecting IVM sensitivity (Figure 4-8).

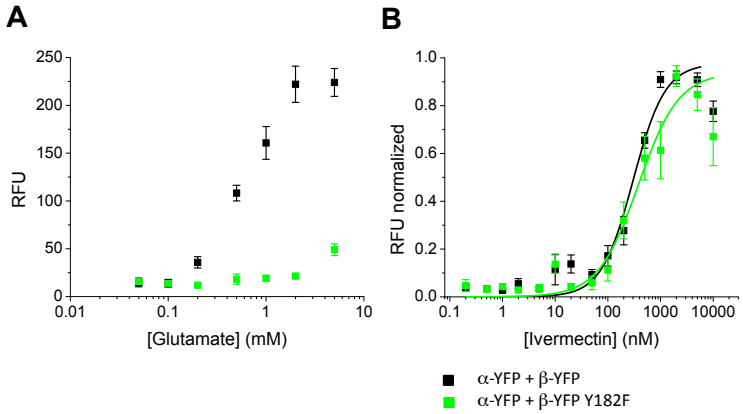

Figure 4-8. Confirmation of the (β)Y182F glutamate insensitive mutation. Glutamate (raw RFU) and IVM (normalized RFU) activation were assayed using the FlexStation. The (β)Y182F mutation renders heteromeric GluCl receptors insensitive to glutamate (*A*) while maintaining sensitivity to IVM (*B*). IVM activation parameters are shown in Table 4-1.

The incompatibility of the (β)Y182F mutation prompted the consideration of alternative mutations to achieve glutamate insensitivity. A recently available crystal structure of GluCl provides the precise molecular interactions of glutamate within the receptor binding site (Figure 4-9A)[36]. Structural coordinates reveal a cation-pi interaction between the electron-rich aromatic ring of a tyrosine residue (Y200 of $GluCl_{cryst}$) and the positively charged amino group of glutamate. This tyrosine residue corresponds to Y261 of the nascent α subunit which aligns with Y232 of the nascent β subunit (note, nascent numbering includes signal peptide residues). Since the resolved structure is comprised of

only α subunits, it is not known which subunit, α or β, provides the principle and complimentary faces of the binding site in the heteromeric receptor. For that reason, the potential cation-pi-forming tyrosine residue of each subunit was mutated to alanine, (α)Y261A and (β)Y232A, and tested individually for glutamate and IVM activation.

The (β)Y232A mutant was successful in abolishing glutamate sensitivity while perfectly maintaining IVM sensitivity (Figure 4-9B, C). The (α)Y261A mutant was also insensitive to glutamate (Figure 4-9E). However, the IVM concentration-response curve for this mutant was right-shifted with a steep Hill coefficient, much like that observed for GluCl α-YFP homomers (Figure 4-9F; see Chapter 3, Figure 3-7). This suggests that the (α)Y261A mutation gives rise to a predominating population of α homomer receptors, which are inherently unresponsive to glutamate binding events. Though not conclusive, these results suggest that β serves as the principle subunit of heteromeric GluCl αβ receptors. To determine if (β)Y232A could function as an alternative glutamate insensitive mutation toward an optimized silencing tool, it was combined with the (α)L9'F mutation. Unfortunately, the high sensitivity component of the biphasic (α)L9'F response was still not maintained (Figure 4-9D).

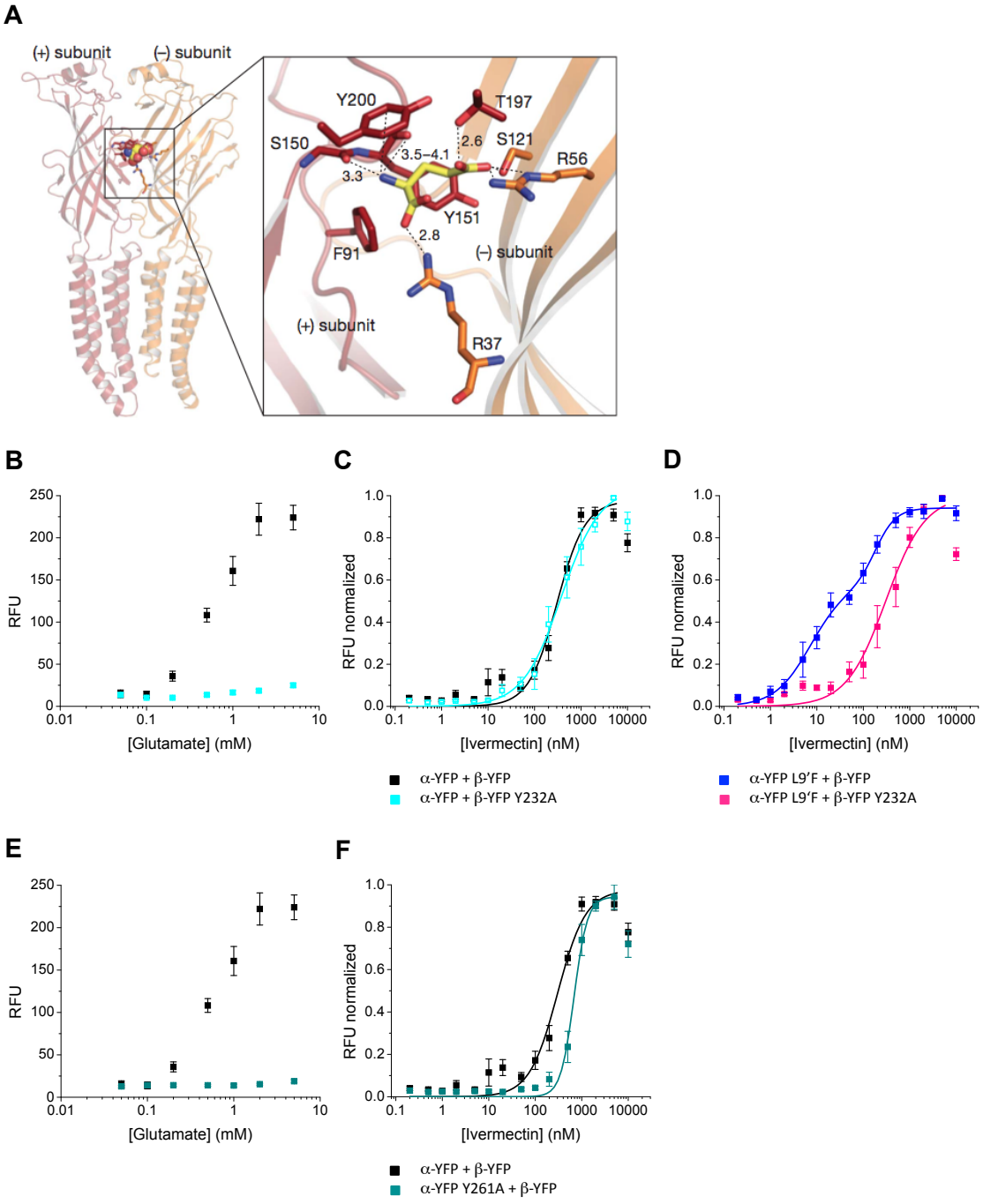

Figure 4-9. An alternative glutamate insensitive mutation still does not maintain high IVM sensitivity. *A.* Glutamate binding interactions with $GluCl_{cryst}$ α homomer. (Figure adapted from Hibbs & Gouaux, 2011.)[36] The Y200 residue forms a cation-pi interaction with the amino group of glutamate. *B–F.* Glutamate (raw RFU) and IVM (normalized RFU) activation were assayed using the FlexStation. *B&C.* The (β)Y232A mutation renders heteromeric receptors insensitive to glutamate while maintaining sensitivity to IVM. *D.* The (β)Y232A mutation still eliminates the high sensitivity component of the (α)L9'F biphasic response. *E&F.* The (α)Y261A mutant receptor is also insensitive to glutamate, but the right-shifted IVM concentration-response curve suggests predominant expression of α homomers which are already insensitive to glutamate. IVM activation parameters are shown in Table 4-1.

XFP tag oligomerization affects IVM sensitivity

Reappearance of the steep, right-shifted IVM concentration-response curve characteristic of the GluCl α-YFP homomers warranted a closer look at the effects of fluorescent protein insertion. A four-way comparison of heteromeric WT-XFP receptors with YFP and CFP tags on either or both subunits shows a right shift from the nontagged WT receptor (Figure 4-10A). Cross-comparison of XFP-tagged and nontagged subunits revealed right-shifted curves only when the fluorescent protein was present in the α subunit (Figure 4-10B). It appears the XFP insertion in the α subunit affects IVM sensitivity of both α homomeric and αβ heteromeric receptors.

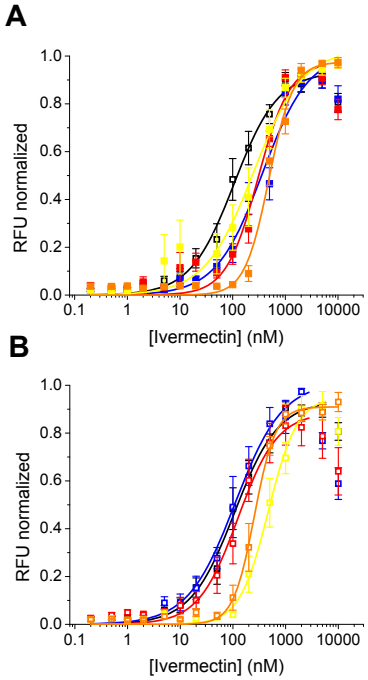

GluCl channel	EC_{50} (μM)	Hill	n
α(WT) + β(WT)	107.14 ± 10.94	1.04 ± 0.09	12
α-YFP + β-CFP	365.20 ± 96.76	0.99 ± 0.16	12
α-YFP + β-YFP	302.08 ± 54.34	1.44 ± 0.27	12
α-CFP + β-YFP	249.59 ± 57.09	0.94 ± 0.15	6
α-CFP + β-CFP	490.25 ± 39.35	1.89 ± 0.24	6
α(WT) + β-CFP	110.26 ± 13.09	0.96 ± 0.08	6
α(WT) + β-YFP	123.85 ± 17.74	1.16 ± 0.15	6
α-YFP + β(WT)	471.85 ± 35.39	1.58 ± 0.14	6
α-CFP + β(WT)	255.72 ± 11.82	2.16 ± 0.17	6

Figure 4-10. The α subunit fluorescent protein (XFP) insertion affects IVM sensitivity. IVM activation was assayed using the FlexStation. *A*. Heteromers with YFP and CFP tags on either or both subunits all show a slight right shift from the nontagged WT receptor. *B*. Heteromers with a YFP or CFP tag on one subunit shows right-shifted curves only when the fluorescent protein is on the α subunit. Ivermectin activation parameters are presented in the corresponding table.

Fluorescent proteins have a tendency to dimerize at high concentrations. A crystal structure of GFP shows a hydrophobic dimer interface comprised of amino acid residues Ala206, Leu221, and Phe223 (Figure 4-11A)[37]. A strictly monomeric form of XFP can be obtained by mutating Ala206 to a Lys residue which introduces a long, positively charged side chain that disrupts the hydrophobic interface[38]. Fluorescent protein dimerization is likely to occur when restricted to two-dimensional space as when fused to membrane proteins[39]. To determine if XFP dimerization was having an effect on channel function or possibly even stoichiometry of GluCl, an A206K mutation was incorporated into the engineered constructs. The IVM concentration-response curve of the wild-type monomeric YFP-tagged (mYFP) receptor was no longer right-shifted compared to the WT receptor, and even revealed a distinctive second component (Figure 4-11B). Incorporation of mYFP into the (α)L9'F receptor produced a more pronounced biphasic relationship than any previously observed. The same extreme biphasic behavior resulted when the L9'F mutation was present in the β subunit or present both α and β subunits (Figure 4-11C). Addition of (β)Y182F to the (α)L9'F mutation with mYFP tags now maintained a high sensitivity component, however the proportion was still reduced (Figure 4-11D).

Due the significant improvement of mYFP, this A206K mutation was combined iteratively with the L9'F mutations, (α)L9'F and/or (β)L9'F, the glutamate insensitive mutations, (β)Y182F or (β)Y232A, and the ER-retention mutation, (β)RSR_AAA, to screen for the greatest increase in IVM sensitivity (Figure 4-12A). This process revealed high sensitivity IVM activation for the initially favored receptor (α-YFP L9'F + β-YFP RSR_AAA) now including a glutamate insensitive mutation and monomeric fluorescent

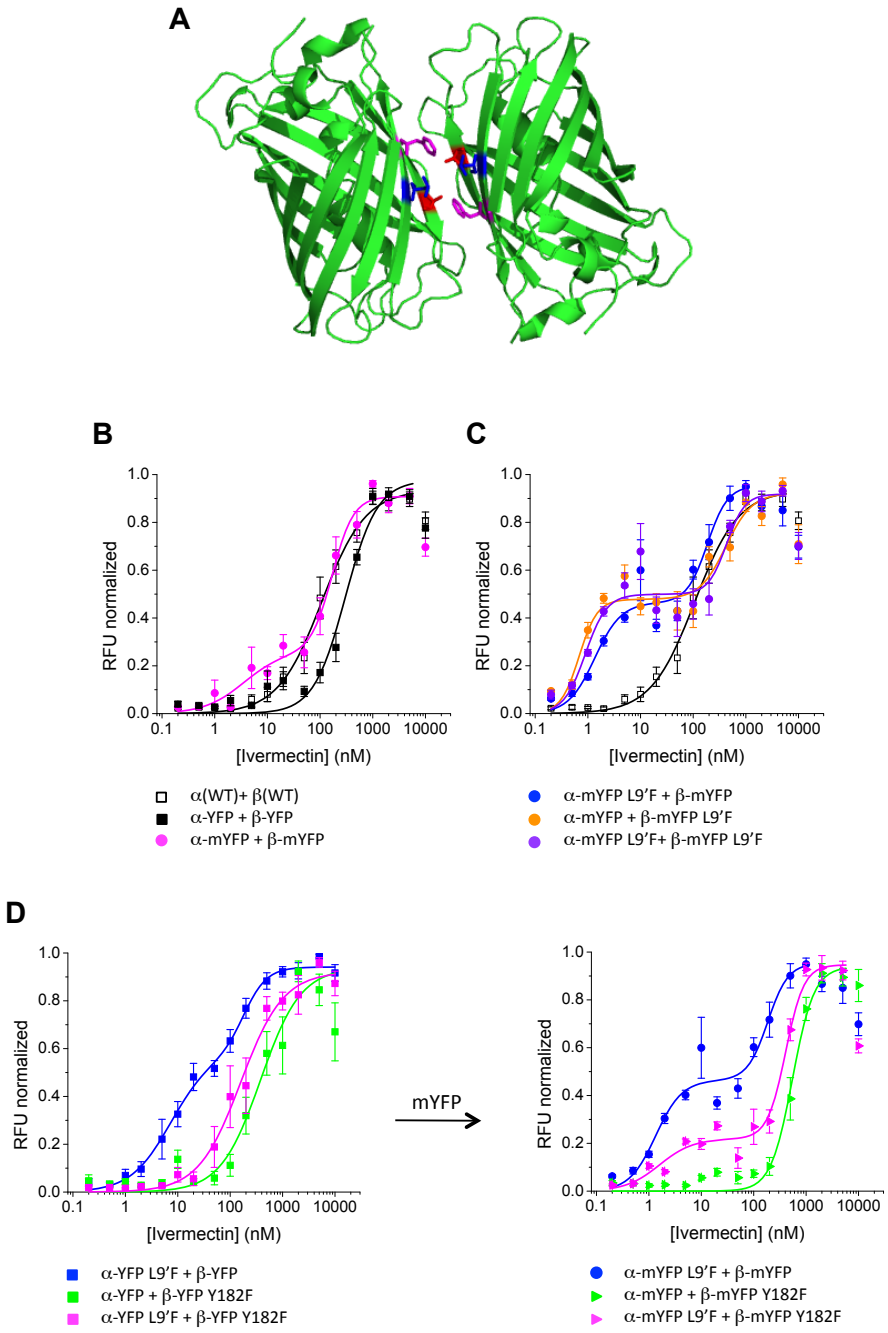

Figure 4-11. Monomeric YFP mutation (A206K) increases high IVM sensitivity component. *A.* Crystal structure of GFP dimer (1GFL.pdb) indicates a hydrophobic interface composed of residues Ala206, Leu221, and Phe223. *B.* Receptors with mYFP tags on both α and β subunits are no longer right-shifted from the nontagged WT receptor. *C.* The incorporation of mYFP enhances the high IVM sensitivity component of the (α)L9'F biphasic curve. An L9'F mutation in the β subunit or in both α and β subunits gives similar results. *D.* The mYFP mutation maintains a high IVM sensitivity component upon addition of the (β)Y182F mutation to (α)L9'F. IVM activation was assayed using the FlexStation. IVM activation parameters are shown in Table 4-1.

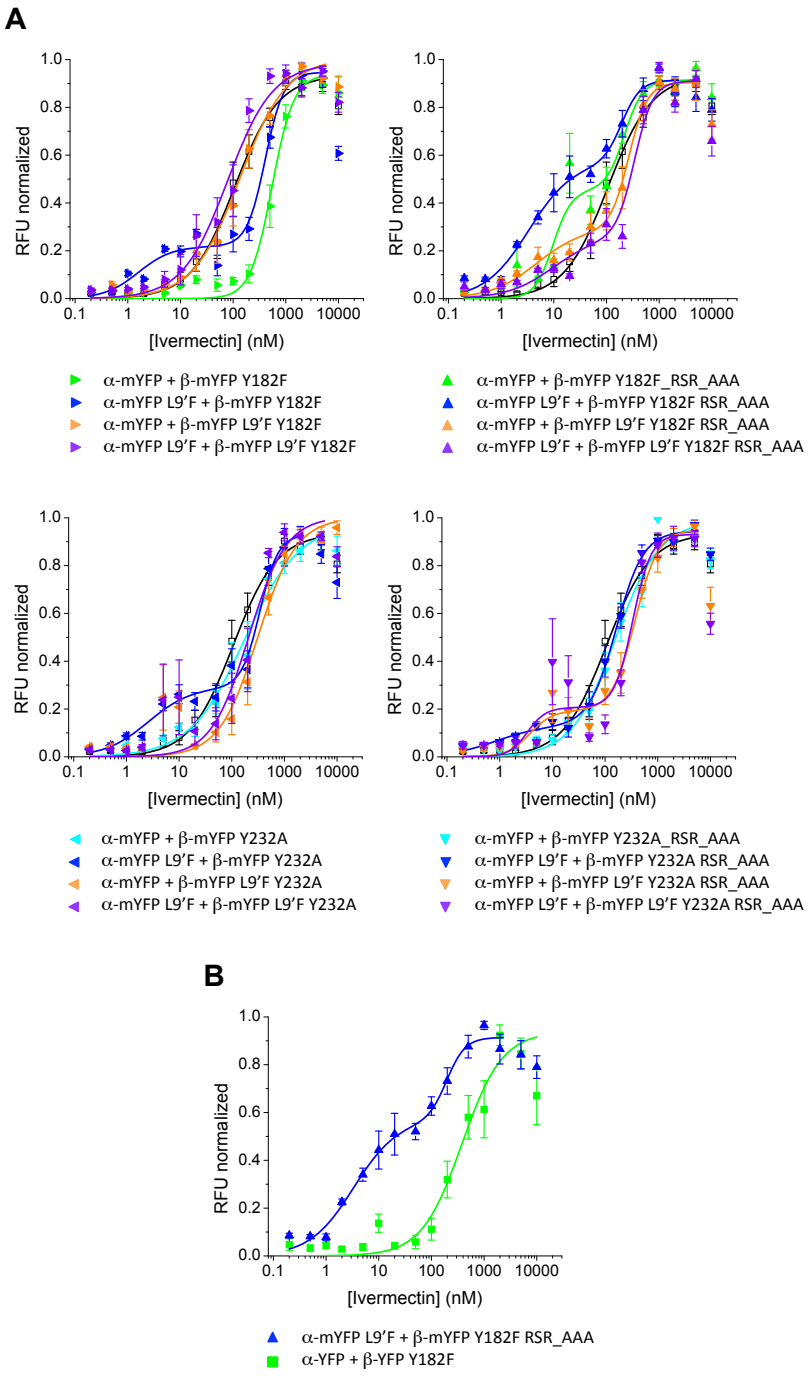

Figure 4-12. Identification of an optimally engineered receptor. IVM activation was assayed using the FlexStation. *A.* Normalized IVM concentration-response curves of mutant receptor combinations including mYFP tags (*all panels*) with the (α)L9'F and/or (β)L9'F mutations (*all panels*), the glutamate insensitive mutations (β)Y182F (*top panels*) and (β)Y232A (*bottom panels*), and the ER-retention mutation (β)RSR_AAA (*right panels*). *B.* GluCl α-mYFP L9'F + β-mYFP Y182F RSR_AAA has the greatest increase in IVM sensitivity compared to the original silencing tool. IVM activation parameters are shown in Table 4-1.

GluCl channel		1st comp	EC_{50} (nM)	Hill	EC_{50} (nM)	Hill	n
α(WT) + β(WT)	□				107.14 ± 10.94	1.04 ± 0.09	12
α-YFP + β-YFP	■				302.08 ± 54.34	1.44 ± 0.27	12
α-YFP + β-YFP RSR_AAA	◆	0.35	8.55 ± 3.16	2.5 ± 1.67	163.15 ± 38.31	2.04 ± 0.84	6
α-YFP + β-YFP RRR_AAA	◆				111.88 ± 9.98	1.44 ± 0.16	6
α-YFP + β-YFP RSR_AAA&RRR_AAA	◆				233.06 ± 17.71	1.44 ± 0.13	6
α-YFP L9'F + β-YFP	■	0.61	7.27 ± 2.85	1.14 ± 0.24	185.35 ± 50.16	1.99 ± 0.82	6
α-YFP L9'F + β-YFP RSR_AAA	■	0.53	3.91 ± 1.69	1.64 ± 0.69	95.28 ± 30.91	2.24 ± 1.27	12
α-YFP L9'F + β-YFP RRR_AAA	■				83.31 ± 21.70	0.94 ± 0.17	6
α-YFP L9'F + β-YFP RSR_AAA&RRR_AAA	■	0.39	2.52 ± 0.83	1.81 ± 0.83	243.71 ± 44.61	2.50 ± 0.98	6
α-YFP + β-YFP Y182F	■				380.41 ± 105.68	1.14 ± 0.24	6
α-YFP L9'F + β-YFP Y182F	■				159.81 ± 20.71	1.07 ± 0.12	6
α-YFP + β-YFP Y182F RSR_AAA	■				365.49 ± 48.35	1.35 ± 0.17	6
α-YFP L9'F + β-YFP Y182F RSR_AAA	■				45.08 ± 5.37	1.21 ± 0.14	6
α-YFP + β-YFP Y232A	■				377.56 ± 44.80	1.04 ± 0.08	6
α-YFP L9'F + β-YFP Y232A	■				304.01 ± 31.67	1.03 ± 0.10	6
α-YFP Y261A + β-YFP	■				682.81 ± 34.37	3.04 ± 0.38	6
α-mYFP + β-mYFP	●	0.29	3.58 ± 3.66	1.16 ± 0.80	170.46 ± 32.61	2.16 ± 0.79	6
α-mYFP L9'F + β-mYFP	●	0.49	1.35 ± 0.47	1.36 ± 0.85	185.58 ± 62.75	2.24 ± 1.65	6
α-mYFP + β-mYFP L9'F	●	0.48	0.68 ± 0.15	2.5 ± 1.25	418.17 ± 165.12	1.75 ± 1.00	6
α-mYFP L9'F + β-mYFP L9'F	●	0.54	0.90 ± 0.24	2.13 ± 1.15	429.33 ± 156.96	2.5 ± 2.00	6
α-mYFP + β-mYFP Y182F	▶				549.07 ± 50.34	2.11 ± 0.35	6
α-mYFP L9'F + β-mYFP Y182F	▶	0.23	1.59 ± 0.85	1.36 ± 0.85	408.08 ± 49.78	2.5 ± 0.65	6
α-mYFP + β-mYFP L9'F Y182F	▶				134.27 ± 19.92	0.97 ± 0.11	6
α-mYFP L9'F + β-mYFP L9'F Y182F	▶				78.38 ± 14.54	1.01 ± 0.15	6
α-mYFP + β-mYFP Y182F RSR_AAA	▲	0.50	9.73 ± 3.98	2.50 ± 2.04	218.57 ± 91.48	2.5 ± 2.47	6
α-mYFP L9'F + β-mYFP Y182F RSR_AAA	▲	0.63	3.35 ± 1.36	1.04 ± 0.27	196.26 ± 49.81	2.5 ± 1.64	6
α-mYFP + β-mYFP L9'F Y182F RSR_AAA	▲	0.33	4.70 ± 2.98	1.00 ± 0.39	265.91 ± 32.59	2.5 ± 0.61	6
α-mYFP L9'F + β-mYFP L9'F Y182F RSR_AAA	▲	0.29	9.92 ± 20.71	1.00 ± 1.12	340.09 ± 103.09	2.5 ± 1.41	6
α-mYFP + β-mYFP Y232A	◀				174.49 ± 38.29	0.83 ± 0.10	6
α-mYFP L9'F + β-mYFP Y232A	◀	0.31	2.61 ± 1.51	1.07 ± 0.48	343.17 ± 52.89	2.5 ± 0.75	6
α-mYFP + β-mYFP L9'F Y232A	◀				311.27 ± 85.60	1.18 ± 0.29	6
α-mYFP L9'F + β-mYFP L9'F Y232A	◀				209.70 ± 69.82	1.22 ± 0.38	6
α-mYFP + β-mYFP Y232A RSR_AAA	▼	0.27	1.81 ± 4.53	1.08 ± 1.88	141.98 ± 69.99	1.73 ± 1.27	6
α-mYFP L9'F + β-mYFP Y232A RSR_AAA	▼	0.36	21.58 ± 53.57	1.00 ± 0.89	277.64 ± 85.65	2.30 ± 1.31	6
α-mYFP + β-mYFP L9'F Y232A RSR_AAA	▼	0.20	3.72 ± 2.11	2.04 ± 1.76	371.81 ± 60.99	1.99 ± 0.54	6
α-mYFP L9'F + β-mYFP L9'F Y232A RSR_AAA	▼	0.22	3.35 ± 3.06	2.5 ± 4.08	333.88 ± 96.74	2.50 ± 1.34	6

Table 4-1. Ivermectin activation parameters for various GluCl mutant receptors. Parameters correspond to concentration-response curves in Figures 4-4A, 4-6A, 4-7A,B,C, 4-8B, 4-9C,D,F, 4-11B,C,D, 4-12A,B. The EC_{50} and Hill coefficient values represent the mean ± SEM for the number of measurements (n) obtained.

protein tags. Thus, the mYFP mutation restored the high IVM sensitivity component previously lost upon addition of (β)Y182F. The optimized GluCl α-mYFP L9'F + β-mYFP Y182F RSR_AAA receptor is more sensitive to IVM than the original receptor silencing tool by ~2 orders of magnitude (Figure 4-12B, Table 4-1).

Biphasic response is not due to potentiation

Every instance of increased IVM sensitivity transpired as part of a biphasic response. The persistent low sensitivity component and the deleterious effect of including a glutamate insensitive mutation on the high sensitivity component were perplexing. With regard to the latter issue, it is conceivable that low (nM) glutamate present in the extracellular fluid could contribute to the high sensitivity component of the IVM response, since the (α)L9'F mutation has increased sensitivity for glutamate in addition to IVM (Chapter 3, Figure 3-6). Furthermore, examples of IVM potentiation of the glutamate response, as well as, glutamate potentiation of the IVM response have both been reported for GluCl[40-42]. If the high sensitivity component of the (α)L9'F biphasic response is due to potentiation by low levels of extracellular glutamate, then a glutamate insensitive mutation would withdraw the effect.

To test this possibility, a complex FlexStation assay was conducted. A large concentration range of glutamate (from 1 nM to 5 mM) was sampled in the presence of 10 nM IVM. This concentration of IVM was chosen to represent high sensitivity activation, and an additional '10 nM IVM only' dose was included for response normalization. This approach probed the possibility of potentiation in both directions, identifying (1) whether low concentrations of glutamate potentiate the 10 nM IVM response, and (2) if the presence of 10 nM IVM potentiates the glutamate response, both at nonactivating and activating concentrations of glutamate.

Using the mYFP-tagged constructs, the WT, (α)L9'F, (β)Y182F, and the combined (α)L9'F + (β)Y182F receptors were assayed. The mean '10 nM IVM only'

response was as expected; the (α)L9'F mutation increases IVM sensitivity and addition of the (β)Y182F mutation abolishes this effect (Figure 4-13A). For each receptor, low glutamate (1 nM to 20 μM) does not potentiate the 10 nM IVM response, as normalization results in a value of 1 (Figure 4-13B). For the (α)L9'F receptor in particular, higher concentrations of glutamate do not increase the magnitude more than that already induced by 10 nM IVM, confirming that extracellular glutamate levels do not influence the high sensitivity component of the biphasic response. Furthermore, a plot of the raw concentration-response relationship of glutamate in the presence of 10 nM IVM is essentially the same as that of glutamate alone (Figure 4-13C). A ratio of the responses at 1 mM glutamate reveals, if anything, that the presence of IVM might slightly recover some glutamate sensitivity of the (β)Y182F mutant receptor, but it does not potentiate the glutamate response of the (α)L9'F mutant receptor (Figure 4-13D).

Biphasic response is due to stoichiometry

A second possible explanation for the biphasic response, discussed in Chapter 3, is a shift in receptor stoichiometry, i.e., a shift in the ratio of α:β subunits in the assembled pentamer. The presence of multiple stoichiometric populations with differing agonist sensitivities can result in a multicomponent concentration-response curve. In FlexStation assays, the expression of GluCl α homomers consistently produces a monophasic curve, while co-expression of α with the β subunit has yielded biphasic concentration-response curves for several receptors, most prominently in the case of individual (α)L9'F and (β)RSR_AAA mutant receptors. For a simple test to determine if stoichiometry could be

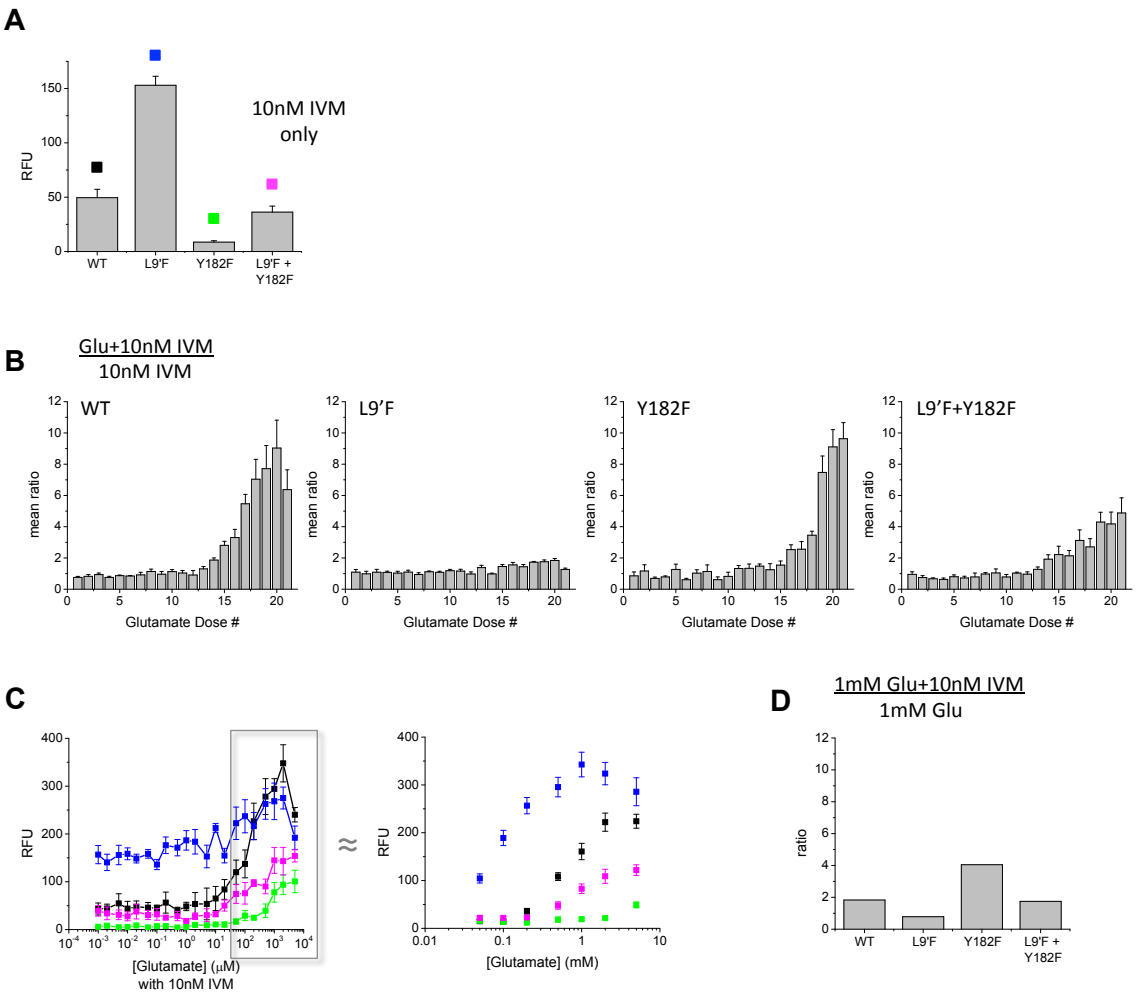

Figure 4-13. Potentiation does not explain the biphasic response of (α)L9'F mutant receptors. IVM activation was assayed using the FlexStation. *A.* Mean response of WT, (α)L9'F, (β)Y182F, and (α)L9'F + (β)Y182F receptors to a '10 nM IVM only' application (for normalization). *B.* Signals of twenty-one increasing concentrations of glutamate in the presence of 10 nM IVM normalized by the '10 nM IVM only' response. Low concentrations of glutamate (1 nM to 20 μM) do not potentiate the 10 nM IVM response. *C.* Raw RFU signal for activating concentrations of glutamate in the presence of 10 nM IVM (last 7 doses) is comparable to that of glutamate alone. *D.* Response ratio for 1 mM glutamate shows 10 nM IVM does not potentiate the glutamate response of (α)L9'F mutant receptors.

responsible for the biphasic response of these two mutant receptors (tagged with mYFP), different ratios of α and β DNA (1:1, 4:1, and 1:4) were transfected into HEK293 cells and assayed on the FlexStation. As previously observed for both cases, a 1:1 ratio

produced a two-component concentration-dependent relationship. Biasing for β (1:4), in general, showed no further increase in IVM sensitivity, while biasing for α (4:1) indeed showed a decrease in IVM sensitivity (Figure 4-14). Therefore, incorporation of the β subunit confers increased sensitivity to IVM, but requires unbiased co-expression with the α subunit for the maximum effect. This confirms multiple receptor populations are contributing to the biphasic concentration-response curve but the stoichiometric identities remain to be determined.

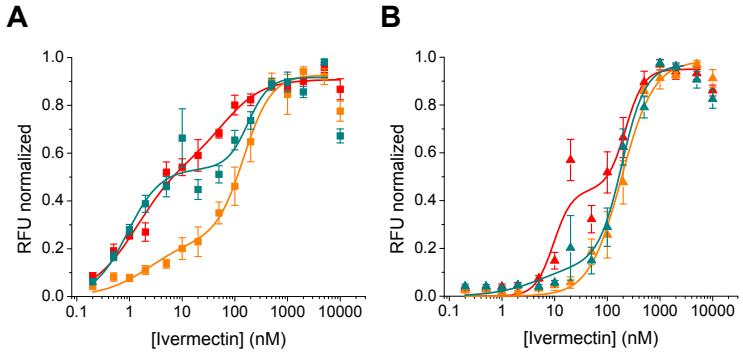

		1st comp	EC_{50} (μM)	Hill	EC_{50} (μM)	Hill	n
■	α-mYFP L9'F + β-mYFP 1:1	0.64	1.37 ± 1.16	1.00 ± 0.40	65.16 ± 70.35	1.17 ± 0.86	6
■	α-mYFP L9'F + β-mYFP 4:1	0.26	2.38 ± 2.64	1.00 ± 0.61	147.24 ± 27.16	1.66 ± 0.42	6
■	α-mYFP L9'F + β-mYFP 1:4	0.58	0.92 ± 0.29	1.39 ± 0.56	178.36 ± 61.16	2.17 ± 1.51	6
▲	α-mYFP + β-mYFP RSR_AAA 1:1	0.47	9.56 ± 3.60	2.50 ± 1.90	220.21 ± 76.06	2.50 ± 2.03	6
▲	α-mYFP + β-mYFP RSR_AAA 4:1				184.22 ± 16.99	1.42 ± 0.15	6
▲	α-mYFP + β-mYFP RSR_AAA 1:4	0.15	5.58 ± 20.08	1.00 ± 1.64	188.88 ± 42.35	1.95 ± 0.78	6

Figure 4-14. Multiple receptor stoichiometries explain the biphasic response. IVM activation was assayed using the FlexStation. *A.* Different ratios of α and β DNA (1:1, 4:1, and 1:4) were transfected into HEK293 cells. The 1:1 ratio (*red*) produced the expected two-component concentration-dependent relationship for (α)L9'F (*panel A.*) and (β)RSR_AAA (*panel B.*) mutant receptors. Biasing for β (1:4, *aqua*) does not further enhance IVM sensitivity. Biasing for α (4:1, *orange*) decreases in IVM sensitivity. Ivermectin activation parameters are presented in the corresponding table.

Retention mutations are not sufficient for β homomer surface expression

The fluorescent protein insertions allow direct visualization and localization of GluCl receptors expressed in a cell. TIRF images of HEK293 cells show GluCl α homomers and αβ heteromers are expressed at the plasma membrane; GluCl β homomers are not (Figure 4-15). Specifically, the α-mYFP subunit shows plasma membrane fluorescence when transfected alone or cotransfected with β(WT). Plasma membrane fluorescence is also observed when the β-mYFP subunit is cotransfected with α(WT). Transfection of the β-mYFP subunit alone, however, displays exclusive ER retention, as indicated by a reticulated pattern of fluorescence and a lack of hair-like filopodia at the periphery. GluCl β-mYFP subunits bearing either the individual RSR_AAA or RRR_AAA mutations, or the double RSR_AAA&RSR_AAA mutation, display a similar fluorescence pattern as seen for the β-mYFP homomer (Figure 4-16). Thus, mutation of the putative ER retention motifs in the β subunit is not sufficient to allow plasma membrane expression of β homomers.

Western blot analysis was performed to determine if the putative ER retention mutations were increasing heteromeric incorporation of the β subunit at the plasma membrane. Receptors composed of untagged α and the different mYFP-tagged β subunits were expressed in HEK293 cells and probed for only β subunit expression using a GFP antibody. Whole-cell lysate analyses suggest slightly increased protein expression levels for mutated β subunits, despite a similar trend in nonspecific staining (Figure 4-17A). Biotinylation of surface exposed receptors indicates no difference in the number of β subunits assembled into pentamers at the plasma membrane (Figure 4-17B). It should

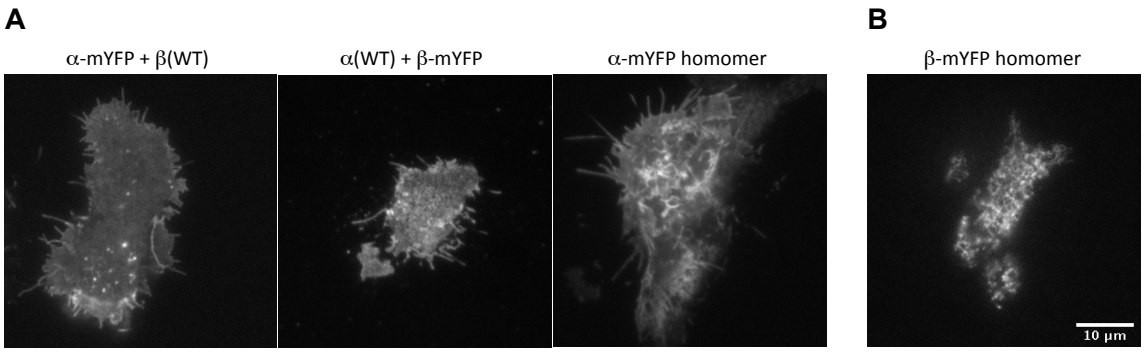

Figure 4-15. GluCl subunit expression in HEK293 cells. *A*. TIRF images show GluCl αβ heteromers and α homomers are expressed at the plasma membrane. The α-mYFP subunit shows plasma membrane fluorescence when transfected alone or cotransfected with β(WT). Plasma membrane fluorescence is also observed when the β-mYFP subunit is cotransfected with α(WT). *B*. GluCl β homomers are not expressed at the plasma membrane. Transfected alone, the β-mYFP subunit displays a reticulated pattern of fluorescence indicative of ER retention and a lack of hair-like filopodia at the periphery.

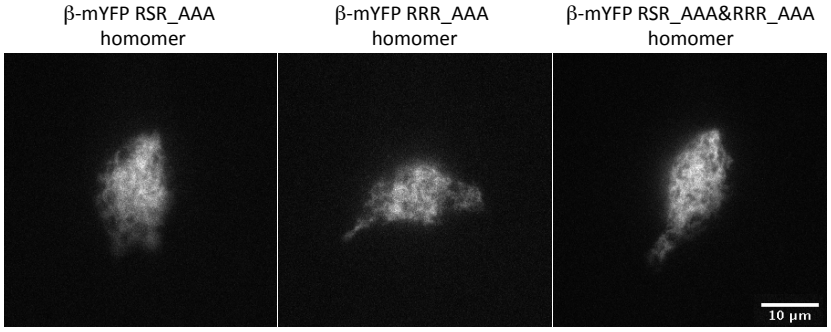

Figure 4-16. GluCl β homomers containing putative ER retention motif mutations still do not exit the ER. TIRF images of HEK293 cells transfected with β-mYFP subunits bearing either the individual putative ER retention motif mutations (RSR_AAA or RRR_AAA) or the double mutation (RSR_AAA&RRR_AAA) show a fluorescence pattern similar to β-mYFP homomers.

be noted that protein bands in these Western blot experiments were visualized by enhanced chemiluminescence with horseradish peroxidase and exposed on radiography film. This method has a limited linear dynamic range so quantification in these instances may be unreliable.

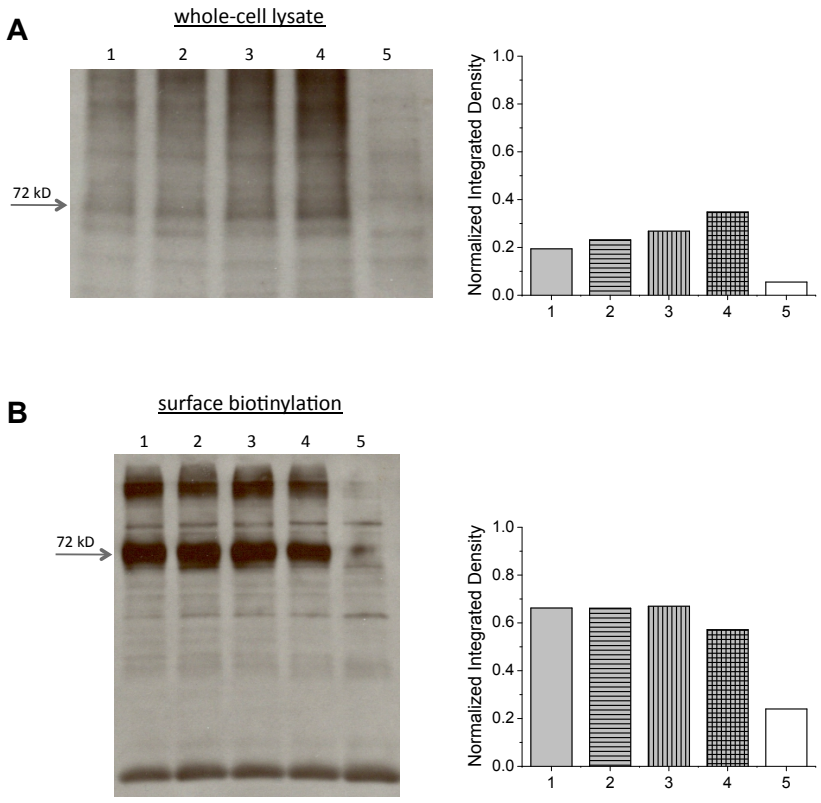

Figure 4-17. Western blot analysis of GluCl β-mYFP subunit expression in HEK293 cells. Quantification of mutated β-mYFP subunits obtained (*A*.) from whole-cell lysate preparations for total protein expression and (*B*.) using a surface biotinylation assay for plasma membrane expression. Protein bands of transferred gels were detected using rabbit anti-GFP primary antibody and goat anti-rabbit HRP secondary antibody. Cells were transfected with the following subunits:

1. α(WT) + β-mYFP
2. α(WT) + β-mYFP RSR_AAA
3. α(WT) + β-mYFP RRR_AAA
4. α(WT) + β-mYFP RSR_AAA&RRR_AAA
5. nontransfected control

RSR mutation increases β subunit expression

HEK293 cells are a convenient system for studying receptor function. However, it is possible that receptor trafficking events in HEK293 cells could be different from that of neurons, especially with respect to stoichiometric preference. Primary neuronal cultures provide a more appropriate environment for *in vitro* experiments. To detect differences in the neuronal expression of GluCl, fluorescently tagged subunits were transfected into embryonic rat hippocampal neurons. Preliminary confocal images in Figure 4-18 illustrate a deficient expression pattern for GluCl β homomers with minimal extension into the processes and comparatively few fluorescent neurons per imaging dish. GluCl α homomers, and various αβ heteromers, on the other hand, exhibit extensive fluorescent projections with no discernable differences. Fluorescence intensity of transfected neurons varies greatly from cell-to-cell within an imaging dish, so direct measure of integrated density is often uninformative. Since neurons have ER compartments throughout much of the length of their processes, it can be difficult to distinguish between receptors retained in the ER and those expressed at the plasma membrane without the use of colocalization markers.

To target only receptors expressed at the plasma membrane, a live cell immunofluorescent surface staining protocol was devised. A V5 epitope tag was added to the C-terminus of both α and β subunits (Figure 4-19A). To ensure that addition of the V5-tags did not disrupt protein folding and pentameric assembly, tagged subunits were assayed for channel function in HEK293 cells using the FlexStation. The V5-tagged constructs formed functional channels similar to WT-mYFP when the V5 tag was present on either α or β subunits. Receptors with V5 tags on both α and β subunits did not show

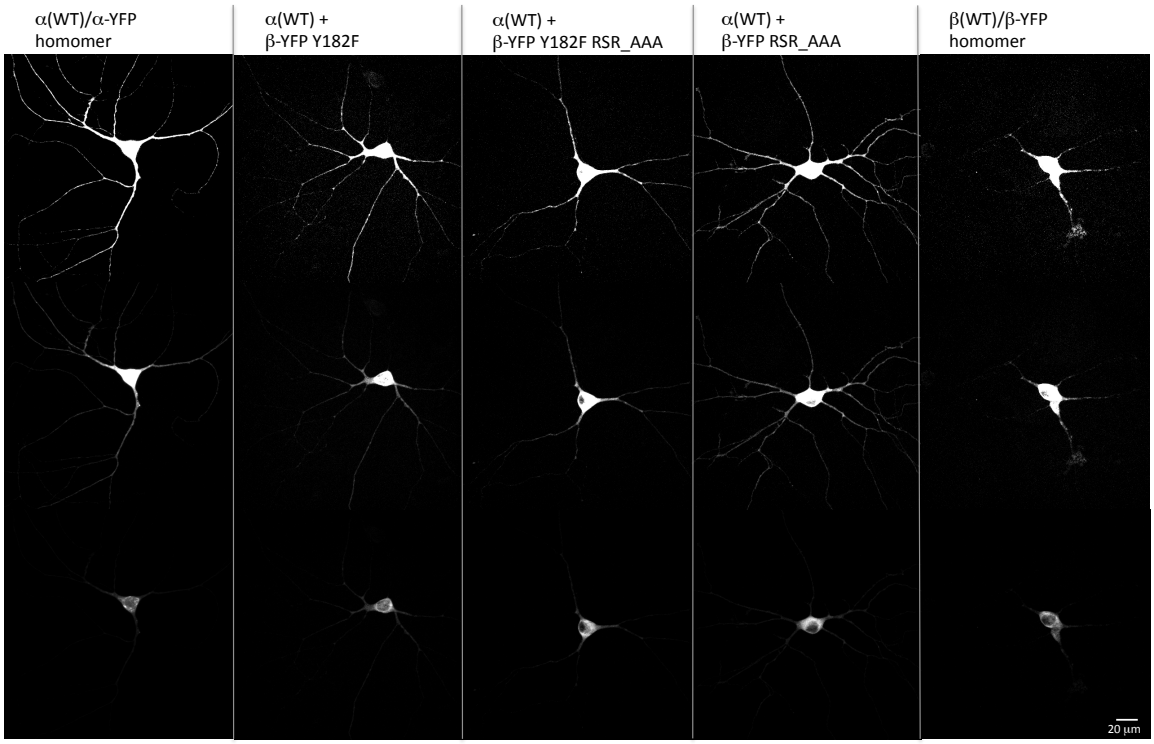

Figure 4-18. Confocal images of transfected rat hippocampal neurons with fluorescent GluCl receptors. Image brightness and contrast was adjusted to compare neuronal processes and soma separately. Extensive fluorescent projections are apparent for GluCl α homomers and various αβ heteromers. A deficient expression pattern is observed for GluCl β homomers with minimal extension into the processes.

a biphasic response, suggesting a slight interference of heteromeric receptor assembly or function with five tagged subunits (Figure 4-19B). Even though inclusion of these penta-tagged receptors would not be critical for data interpretation in the following experiment, they were sampled for the sake of completeness.

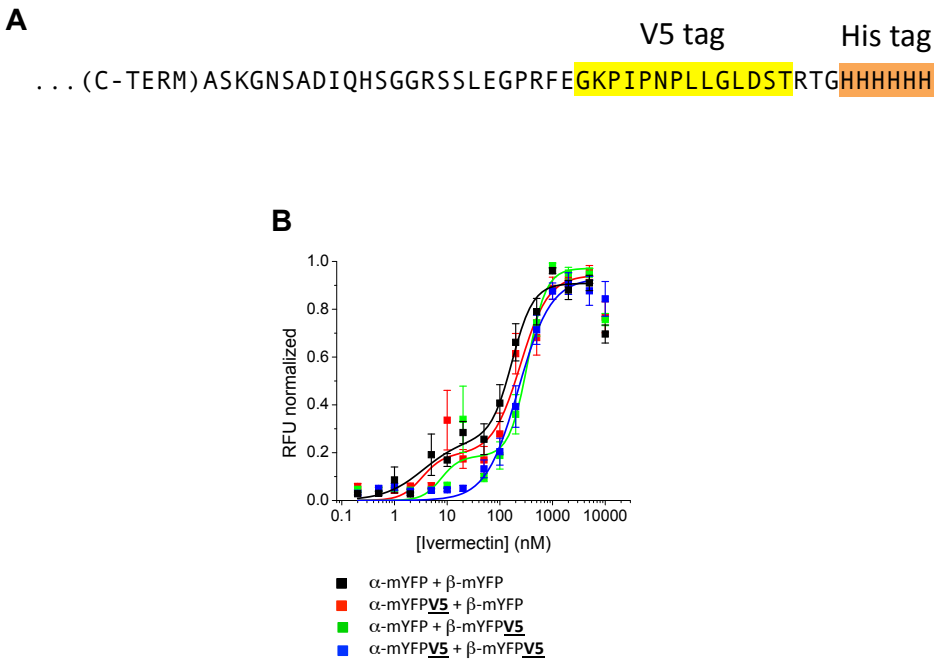

Figure 4-19. Addition of a C-terminal V5 epitope tag does not disrupt pentameric assembly and function. *A*. The V5 epitope tag (also including a 24-residue linker and a 6-His tag; see Materials and Methods) was added to the C-terminus of both α and β subunits. *B*. Fluorescently labeled heteromeric receptors with V5 tags present on either α or β (*red and green*) show a normalized IVM concentration-response curve similar to WT-mYFP. Receptors with V5 tags on both α and β subunits (*blue*) did not show the same two-component response, but had comparable functionality. IVM activation was assayed using the FlexStation.

Rat hippocampal cultures were transfected with α-mYFP and β-mYFP bearing a V5 tag on either or both subunits for three heteromeric receptor conditions: GluCl α-mYFPV5 + β-mYFP, GluCl α-mYFP + β-mYFPV5, and GluCl α-mYFPV5 + β-mYFPV5. Surface exposed receptors were labeled with anti-V5 primary and fluorescent Alexa 555-conjugated secondary antibodies for confocal imaging. Yellow fluorescence contributed by both subunits (mYFP) represented total protein expression, including receptors remaining in subcellular compartments and expressed at the plasma membrane. Red fluorescence from live cell immunostaining (Alexa 555) labeled only subunits

expressed at the cell surface. Red and yellow fluorescent images were acquired as z-stacks and examined for colocalization on a pixel-by-pixel basis. The intensity correlation between a pair of pixels was scored by calculating the normalized mean deviation product (nMDP, see Methods) and visualized on a color scale. Values range from −1 to 1, with values less than zero representing exclusion in cold colors, and values greater than zero signifying colocalization in hot colors (Figure 4-20A). Thus, for a given pixel, a perfect nMDP value of 1 indicates that maximum intensity yellow fluorescence is colocalized with maximum intensity red fluorescence. An nMDP value of −1 results when a pair of pixels contains maximum fluorescence intensity of one color and zero fluorescence intensity for the other color. An nMDP value of zero denotes black background. All pixels including and deviating from these extremes can be represented by a histogram (Figure 4-20B). Colocalization is evidenced by all positive nMDP values ($0< x \leq 1$) and occurs only for receptors expressed at the surface. Hence, greater nMDP values indicate a greater amount of GluCl expression at the plasma membrane.

The average of all positive nMDP values represents total surface expression levels of receptor (note, surface expression levels are not well represented by the sum of all positive nMDP values as the sum is distorted by the size and number of cells imaged). Heteromeric receptors show the same level of surface expression regardless of whether the V5 tag was on the α or β subunit (Figure 4-21A). Lower values were observed when V5 tags were on both subunits, suggesting either lower expression levels or inefficient labeling of all subunits. Transfection of individual V5-tagged subunits corroborated the previous HEK293 cell observations that α homomers are expressed at the plasma membrane of neurons at levels comparable to αβ heteromers, but that β homomers are

not. Heteromeric receptors bearing putative ER retention mutations were assayed in the same format (Figure 4-21B). Incorporation of the (β)RRR_AAA or the double (β)RSR_AAA&RRR_AAA mutations resulted in lower surface expression levels but in a similar manner as WT-mYFP (i.e., less expression when V5 tags are on both α and β subunits). Receptors with the (β)RSR_AAA mutation had the same surface expression levels as WT-mYFP receptors, but in this case, levels were not reduced when V5 tags were on both α and β subunits.

A comparison of the average number of nMDP = 1 values shows that a greater number of maximally correlated pixels occur with V5-tagged α than V5-tagged β when WT and the (β)RRR_AAA and (β)RSR_AAA&RRR_AAA mutant receptors are expressed as heteromers (Figure 4-21C). The average number of nMDP = 1 values is again low when the V5 tag is present on both subunits for these receptors. The (β)RSR_AAA heteromeric receptors, on the other hand, show the opposite result. Maximal colocalization occurs more often for V5-tagged β than V5-tagged α, and the average number of nMDP = 1 values is high when the V5 tag is present on both subunits. Altogether, immunofluorescent results suggest that mutation of the putative β subunit RSR ER retention motif does not increase the total number of receptors trafficked to the plasma membrane, but it may increase the number of β subunits incorporated into the pentamer, shifting the stoichiometric ratio of assembled receptors.

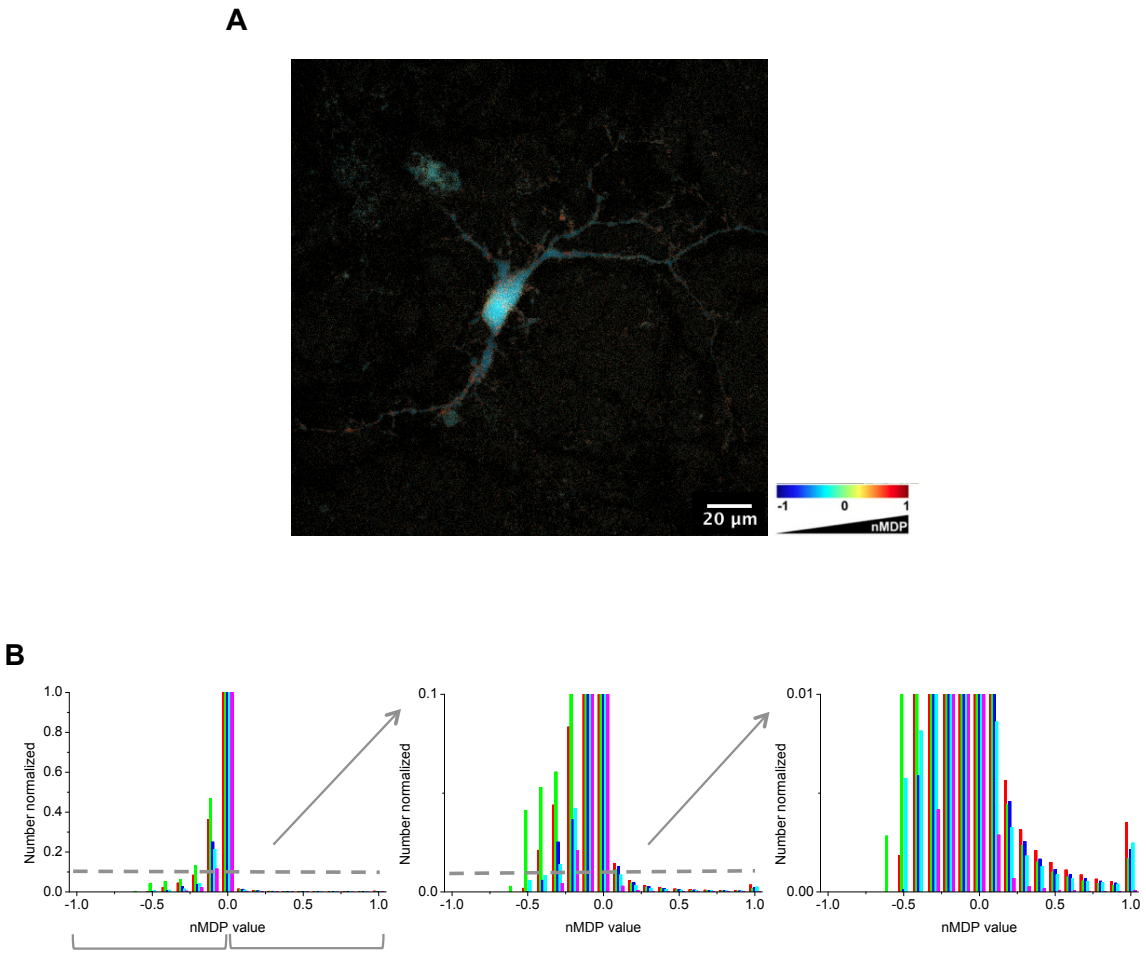

Figure 4-20. Colocalization of immunofluorescent surface staining and intrinsic mYFP fluorescence of GluCl. *A*. Confocal image of GluCl α-mYFPV5 + β-mYFP viewed with the colocalization color scale. (All subunits are fluorescently labeled; only the α subunits expressed at the surface are immunostained.) An nMDP correlation value is calculated for each pixel based on fluorescence intensity. Values range from −1 to 1. Colocalization is shown in hot colors (nMDP > 0); Exclusion is shown in cold colors (nMDP < 0). *B.* Sample histogram of nMDP values. The y-axis is zoomed in for each panel. All positive nMDP values (representing colocalization) indicate expression levels at the surface. Colored bars reflect constructs in Figure 4-21.

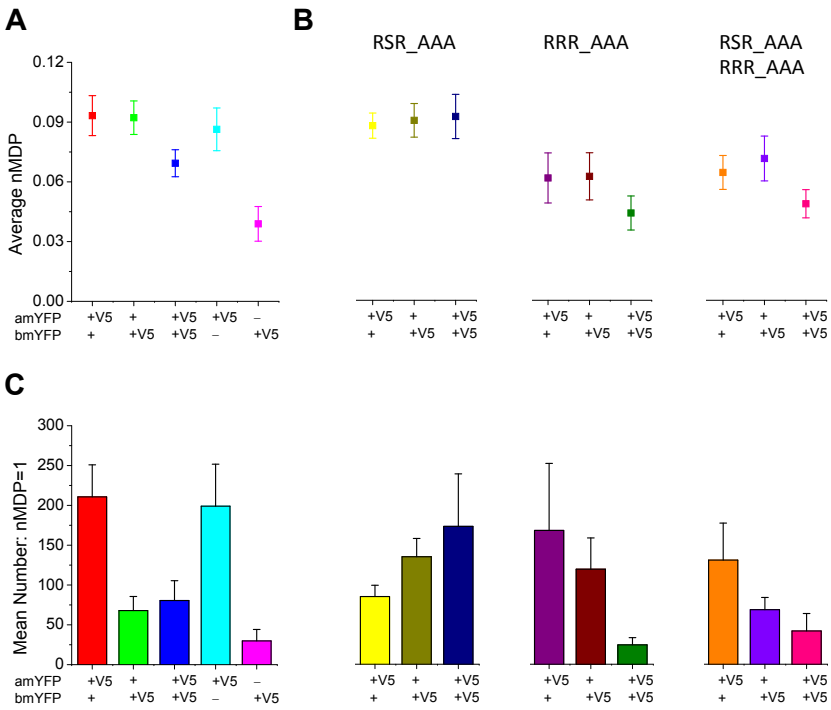

D

	GluCl channel	n cells
■	α-mYFP**V5** + β-mYFP	41
■	α-mYFP + β-mYFP**V5**	49
■	α-mYFP**V5** + β-mYFP**V5**	47
■	α-mYFP**V5** homomer	31
■	β-mYFP**V5** homomer	11
■	α-mYFP**V5** + β-mYFP RSR_AAA	73
■	α-mYFP + β-mYFP RSR_AAA**V5**	50
■	α-mYFP**V5** + β-mYFP RSR_AAA**V5**	34
■	α-mYFP**V5** + β-mYFP RRR_AAA	21
■	α-mYFP + β-mYFP RRR_AAA**V5**	20
■	α-mYFP**V5** + β-mYFP RRR_AAA**V5**	12
■	α-mYFP**V5** + β-mYFP RSRRRR_AAA	21
■	α-mYFP + β-mYFP RSRRRR_AAA**V5**	15
■	α-mYFP**V5** + β-mYFP RSRRRR_AAA**V5**	19

Figure 4-21. The RSR_AAA mutation increases β subunit surface expression but not total receptor surface expression. Confocal colocalization analysis of surface labeled receptors. *A*. Average of all positive nMDP values represents total surface expression levels. GluCl α homomers are expressed at the plasma membrane, β homomers are not. The same level of heteromer surface expression was obtained regardless of whether the V5 tag was on the α or β subunit. Lower expression was observed when V5 tags were on both subunits. *B*. Receptors bearing putative ER retention motif mutations do not increase total receptor surface expression compared to V5-tagged WT (*panel A*.). *C*. Average number of nMDP = 1 values indicates more maximally correlated pixels occur with V5-tagged α than V5-tagged β when WT, RRR_AAA, and RSR_AAA&RRR_AAA receptors are expressed as heteromers. The RSR_AAA mutant receptor shows more maximal colocalization with V5-tagged β subunit than V5-tagged α, suggesting a shift in stoichiometry. *D*. Legend of constructs indicated by color and the number of cells sampled for each.

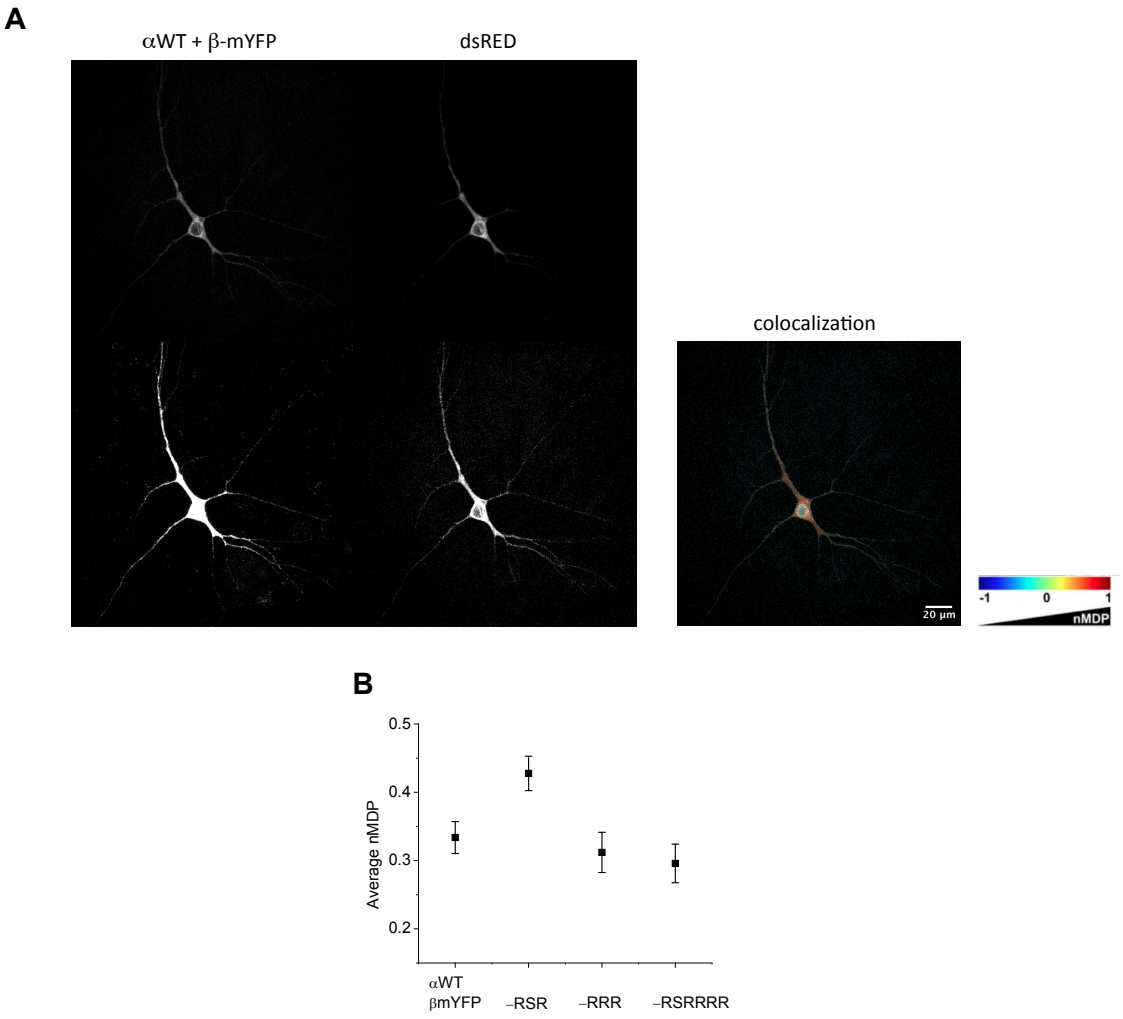

Figure 4-22. The RSR_AAA mutation increases the amount of β subunit in the ER. *A*. Confocal images of GluCl α(WT) + β-mYFP and dsRED (ER marker) viewed independently and with colocalization color scale. Image brightness and contrast was adjusted to compare neuronal processes and soma separately. *B*. Average of all positive nMDP values represents the extent of β subunit localization in the ER. Mutation of the (β)RSR motif probably prevents ER-associated degradation of the β subunit.

Newly synthesized, improperly folded, or unassembled Cys-loop subunits remaining in the ER are degraded rapidly[43-47]. Mutation of an ER retention motif may influence subunit degradation. To determine the relative amounts of WT and mutated β subunits remaining in the ER, a similar pixel-by-pixel colocalization analysis was used.

Rat hippocampal neurons were cotransfected with α(WT) and various β-mYFP subunits along with the fluorescent ER marker, dsRED. Once again, the (β)RSR_AAA mutant was significantly different from WT, (β)RRR_AAA and (β)RSR_AAA&RRR_AAA receptors, showing increased colocalization with ER marker (Figure 4-22). This suggests that the β-mYFP RSR_AAA subunit is not being degraded at the same rate as β-mYFP, leaving more available for heteromeric assembly with α subunits.

An optimized neuronal silencing tool

Mutational screening in HEK293 cells lead to an engineered receptor with increased sensitivity to IVM. Functional data implied that the (β)RSR_AAA mutation increases β subunit incorporation in HEK293 cells and imaging experiments confirmed this mutational effect in neurons. To determine if the newly engineered GluCl α-mXFP L9'F + β-mXFP Y182F RSR_AAA receptor is indeed an improved silencing tool over the original α-XFP + β-XFP Y182F receptor, *in vitro* recordings of IVM-induced spike inhibition were obtained from rat hippocampal neurons. Initially, gap-free recordings were acquired in current clamp mode with bath perfusion of IVM. Continuous recordings were interrupted by two current-injection step protocols, (-100 to 250 pA, 25 pA increments), one following two minutes of bath solution (baseline) and the other after 5 min of 5 nM IVM perfusion. Spontaneous spiking varied from zero to high frequency bursts for transfected and nontransfected neurons. A decrease in spike frequency was not always observed within the duration of IVM application, but greater current injection was often required for spike generation following IVM perfusion (Figure 4-23A).

Several concerns were associated with the bath perfusion protocol including inherent spike variability and run-down effects from internal solution exchange. It also required large solution volumes and the ability to maintain seal resistance for an extended period of time (~10 minutes). Furthermore, variations in real-time silencing may not accurately depict improved sensitivity since it may require up to 15 minutes to achieve full spike inhibition by IVM[1]. For that reason, an alternative pre-incubation procedure was used to ensure adequate time for IVM activation and to avoid submitting patched neurons to lengthy perfusions. Cultured neurons were incubated with 0, 1, or 20 nM IVM for 15 minutes at 37°C/5% CO_2, washed and then recorded for a V-I relationship using the current-injection step protocol (Figure 4-23B and 4-24A). Nontransfected neurons were not influenced by the presence of IVM and construct expression itself had no effect on resting membrane potential (Figure 4-24C). The newly engineered GluCl α-mYFP L9'F + β-mYFP Y182F RSR_AAA receptor shows a significant increase in conductance (as determined by the inverse slope, Figure 4-24D) and a lower mean spike count (Figure 4-24B) for both 1 nM and 20 nM IVM compared to the original α-YFP + β-YFP Y182F silencing tool. Thus, GluCl α-mXFP L9'F + β-mXFP Y182F RSR_AAA, is an optimized construct for IVM-induced spike inhibition.

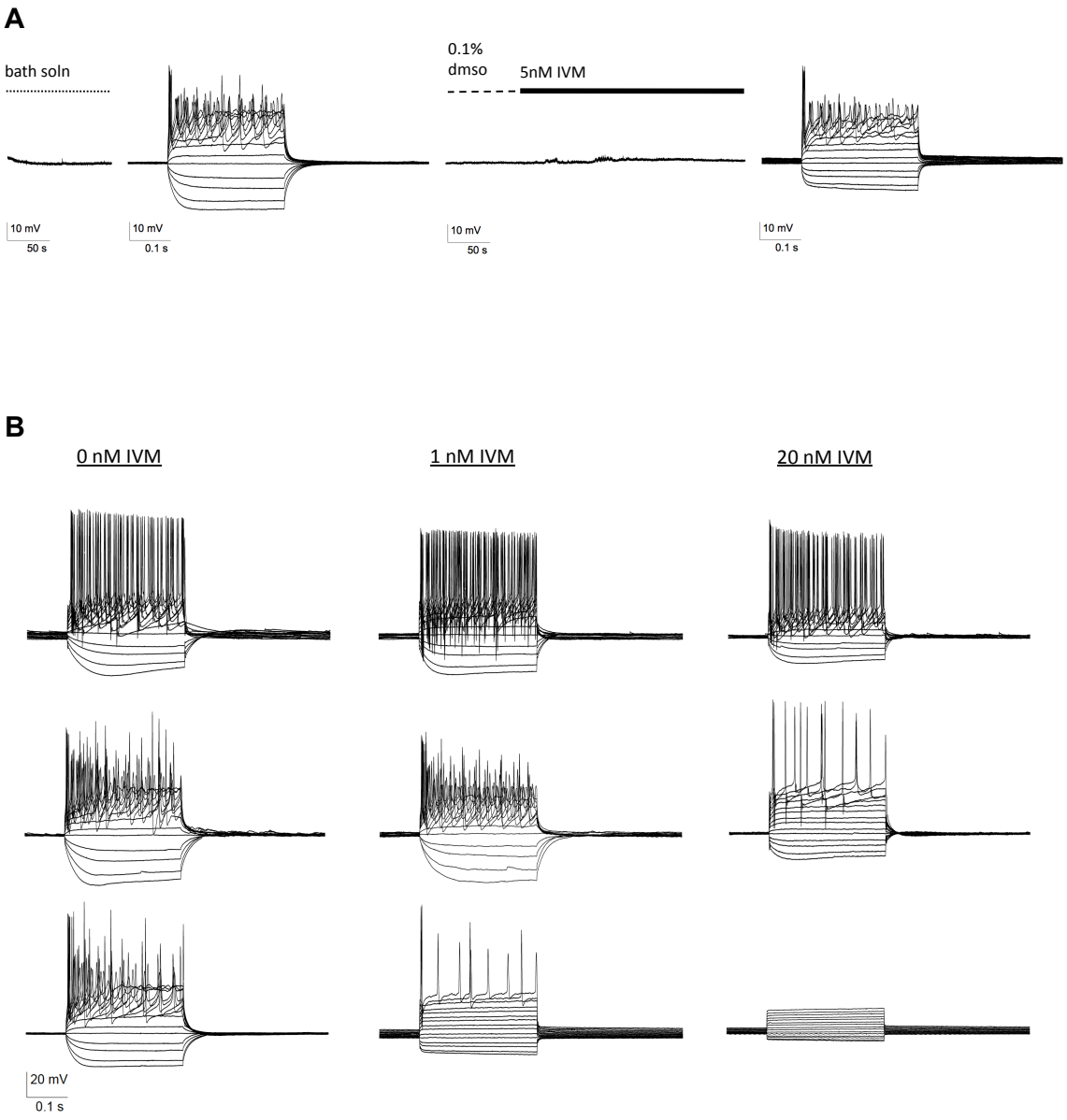

Figure 4-23. Protocols for neuronal silencing by GluCl/IVM *in vitro*. Current clamp recordings of rat hippocampal neuron firing were obtained in response to depolarizing current pulses (-100 to 250 pA, 25 pA increments). *A*. Continuous recording with IVM bath perfusion was a suboptimal method for comparative silencing effects. The neuron depicted was expressing the original silencing tool. (This neuron did not exhibit spontaneous firing.) *B*. A 15-minute pre-incubation of 0, 1, or 20 nM IVM better elucidated a concentration-dependent silencing effect. The optimized construct (α-mYFP L9'F + β-mYFP Y182F RSR_AAA; *bottom panel*), is more sensitive to IVM than the original silencing tool (α-YFP + β-YFP Y182F; *middle panel*), and nontransfected control neurons (*top panel*).

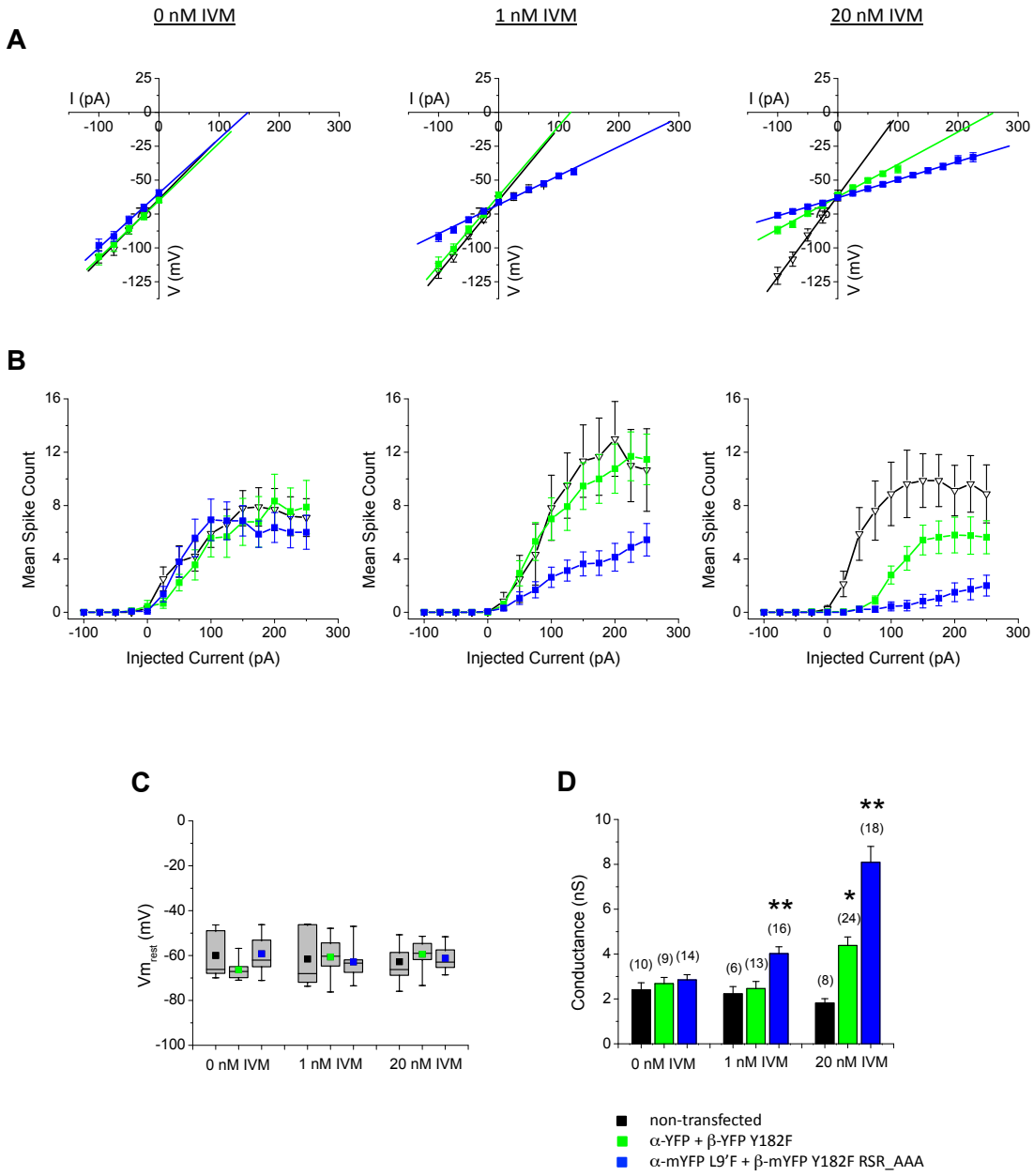

Figure 4-24. An optimized neuronal silencing tool. Current clamp recordings of rat hippocampal neuron firing in response to depolarizing current pulses (-100 to 250 pA, 25 pA increments) were obtained following a 15-min pre-incubation of 0, 1, or 20 nM IVM. *A*. V-I plots from neuronal cultures transfected with the optimized construct (α-mYFP L9'F + β-mYFP Y182F RSR_AAA) were compared to the original construct (α-YFP + β-YFP Y182F) and nontransfected neurons. The optimized receptor exhibits lower slope resistance at 1 and 20 nM IVM. *B*. The optimized receptor also reduced mean evoked spike counts at 1 and 20 nM IVM. *C*. Neither construct expression or the presence of IVM alone significantly altered the resting membrane potential. *D*. The optimized receptor induces a significant increase in conductance (determined by the inverse slope) at both 1 and 20 nM IVM compared to the original silencing tool.

Discussion

Previous reports state that both α and β subunits are required for neuronal silencing by IVM *in vitro* and *in vivo*[1,13]. Variability in GluCl channel expression levels, particularly with the β subunit, appeared responsible for whether or not an individual neuron was inhibited by IVM. It turns out that functional IVM-sensitive α homomers are also expressed at the plasma membrane and that enhanced β subunit incorporation can increase IVM sensitivity. A mixed presence of heteromeric and homomeric receptors within individual neurons may account for the observed variations in spike suppression.

The original GluCl silencing tool has been re-engineered, introducing three new amino acid modifications: the (α)L9'F and (β)RSR_AAA mutations increase IVM sensitivity, probably by altering receptor stoichiometry; the monomeric XFP mutation helps maintain the increased IVM sensitivity upon reintroduction of a glutamate insensitive mutation by relieving the adverse effects of fluorescent protein oligomerization on receptor stoichiometry and function.

Mechanisms of the optimized receptor

In Chapter 2, experiments involving (α)L9'F homomers and heteromers show incorporation of the β subunit significantly increases sensitivity to IVM. The transfection ratio experiment of the current study not only substantiates this claim, but also implies that the (α)L9'F mutation prefers or possibly promotes β subunit incorporation. Biasing for α subunit expression with a 4α:1β ratio still yields a two-component IVM

concentration-response curve for this mutant. Even the low sensitivity component of this curve (EC_{50} = 150 nM) is more sensitive than that of (α)L9'F homomers (EC_{50} = 450 nM). According to one theory of Cys-loop receptor assembly, subunits initially dimerize then two dimers subsequently incorporate a fifth subunit to form an assembled pentamer (reviewed in[48]). The (α)L9'F mutation may either promote α-β dimerization or hinder α-α dimerization by means of intermolecular forces or steric preferences, resulting in a predominantly heteromeric αβ receptor population including more β subunits per assembled receptor.

The fluorescent fusion proteins YFP and CFP are interchangeable between α and β subunits. However, presence of an XFP insertion in the α subunit reduced the IVM sensitivity of both α homomers and αβ heteromers compared to nontagged receptors, suggesting an interference with receptor function. Introduction of an A206K mutation for monomeric XFP alleviated this reduction. The mXFP tag also introduced a modest high IVM sensitivity component for the heteromeric nonmutant receptor and further enhanced the high sensitivity component of the heteromeric (α)L9'F mutant receptor, implying XFP oligomerization affected stoichiometry as well.

The β subunit requires masking of an arginine-based ER retention motif by co-assembly with the α subunit to exit the ER; β homomers are not trafficked to the plasma membrane. In the presence of α, the (β)RSR_AAA retention mutation increases the amount of β at the plasma membrane. The (β)RSR_AAA mutation also elevates β subunit levels in the ER, indicating that it does not simply enhance β subunit surface expression by reducing ER retention. Mutation of putative ER retention motifs alone

were not sufficient to allow surface expression of β homomers, suggesting an additional unknown quality control motif is likely involved in the retention mechanism. Instead, the (β)RSR_AAA mutation probably impedes ER-associated degradation of the β subunit, either directly, by preventing targeted degradation thereby prolonging its availability for α-β dimerization, or indirectly, by facilitating stable α-β dimer formation consequently preventing its degradation. Either way, the (β)RSR_AAA mutation promotes heteromeric receptor assembly evident by the biphasic IVM concentration-response curve. Though it is clear that α homomers are capable of forming functional channels at the plasma membrane, it is unknown to what extent their presence is maintained when β subunits are available. Limiting β subunit degradation may keep α homomer expression to a minimum. A reduced level of α subunit surface expression was confirmed with the (β)RSR_AAA mutation, however, it cannot be determined if the prevalence of α homomer expression was reduced or if the stoichiometry of αβ heteromeric expression was simply shifted to include fewer α subunits per assembled receptor.

Contrary to initial functional assays on the FlexStation, the (β)RSR_AAA mutation does not increase total surface expression. The magnitude of RFU signal from the FlexStation can be influenced by a number of variables, including cell density in the well, transfection efficiency, receptor expression levels, and changes in receptor efficacy and should therefore be interpreted with caution. Like the (α)L9'F mutation, the (β)RSR_AAA mutation gives rise to a biphasic IVM concentration-response, but a monophasic glutamate concentration-response. Though the (α)L9'F and (β)RSR_AAA mutations may not provide a homogeneous receptor population, the populations present have significantly increased IVM sensitivity compared to that of the original silencing

tool, likely eliminating a major contributing factor of suboptimal firing inhibition. During *in vitro* recordings, variability in spike suppression was observed from cell-to-cell with both the original and optimized receptor tools, but was comparable to the variable number of evoked spikes observed from a nontransfected cell. Smaller error bars in the mean spike counts suggest reduced variability in spike suppression with the optimized receptor.

Biphasic curves are due to shifts in stoichiometry

As mentioned, the biphasic concentration-response curve observed with heterologous expression of the optimized GluCl receptor in HEK293 cells is probably the result of multiple receptor populations. Other subunits of the Cys-loop receptor family are known to exist in multiple stoichiometries. For example, α4β2 nicotinic acetylcholine receptors (nAChRs) form two stoichiometric populations with subunit ratios of 2α:3β and 3α:2β constituting high and low sensitivity receptors, respectively[49-51]. The glycine receptor (GlyR), which is the closest mammalian homolog to GluCl, forms functional channels as α homomers and αβ heteromers in mammalian expression systems[52]. The α homomers predominate during embryonic and neonatal development while heteromeric αβ GlyRs exist in the adult[53], though the precise heteromeric stoichiometry, 3α:2β[54] or 2α:3β[55], has been debated.

It is not clear if the stoichiometric GluCl populations present in HEK293 cells coincide with those present in neurons. IVM concentrations required for GluCl activation in HEK293 cells are higher than that required for silencing in neurons. According to the

FlexStation assays of the current study, the IVM EC_{50} for αβ WT GluCl in HEK293 cells is around 100 nM. In neurons, the EC_{50} for IVM-induced conductance measurements of αβ WT GluCl was reportedly 1.3 nM[12]. The time allowed for IVM activation and the method of detection certainly influences these measurements. For example, this ~1 nM IVM EC_{50} can be achieved in HEK293 cells for the WT receptor following lengthy (1 hour) pre-incubation with low concentrations of IVM (see Chapter 5, Figure 5-3). The ~1 nM EC_{50} also corresponds with the high sensitivity component of optimized receptor activation in HEK293 cells, observed as an increasingly robust signal within seconds to minutes. Discrepancies in IVM EC_{50} could be dependent on cell-type with different preferences for receptor stoichiometry or different posttranslational modifications that alter receptor activation. For example, homogeneous receptor populations can often be obtained by biasing transfection ratios in *Xenopus* oocytes[49]. Attempts to bias GluCl subunit expression in HEK293 cells did alter the shape of the IVM concentration-response but did not produce a monophasic high sensitivity curve. Mammalian cells likely possess cell-specific machinery for more regulated receptor trafficking compared to *Xenopus* oocytes. Similarly, neurons may possess alternative posttranslational processing and regulatory mechanisms than standard mammalian cell lines.

Implications of the glutamate insensitive mutation

The (α)L9'F gain-of-function mutation facilitates β subunit incorporation to substantially increase heteromeric GluCl αβ sensitivity to IVM. Reintroduction of a glutamate insensitive mutation, either (β)Y182F or (β)Y232A, to the (α)L9'F mutant eliminated the

increase in IVM sensitivity. Whether this attenuation was an actual defect of structure-function or a consequence of altered stoichiometry is unclear. Mutation of the L9' residue is known to directly impact channel gating. The glutamate insensitive mutations are located within the glutamate binding site of the extracellular domain, some 60 Å away from the (α)L9'F mutation at the channel pore. Some residues at or near the binding site serve as gating pathway residues, engaging in long-range functional coupling to transmit binding events to the channel gate. Mutation of such a residue in combination with an L9' mutation can produce a nonmultiplicative EC_{50}, indicating the distant residues are functionally coupled[56]. Evaluation of the glutamate insensitive mutations by mutant cycle analysis in this case is complicated by the biphasic IVM concentration-dependence (i.e., two EC_{50} values) of the (α)L9'F mutation. Alternatively, mutations at or near the glutamate binding site which is positioned at subunit interfaces, could conceivably affect heteromeric subunit assembly. In this instance, the (β)Y182F or (β)Y232A mutations would be preventing efficient incorporation of the β subunit to eliminate the high IVM sensitivity component of the (α)L9'F mutant. The (α)Y261A mutation, which resulted in a predominantly α homomer population, supports the notion that mutations in this region can affect heteromeric receptor formation. Restoration of the high IVM sensitivity component by the mYFP mutation further supports that an altered subunit stoichiometry is responsible for the counteracting effects of the glutamate insensitive and (α)L9'F mutations.

Combining the (α)L9'F mutation with the (β)Y182F glutamate insensitive mutation did recover some glutamate sensitivity in the concentration range tested, generating concern that this could allow constitutive silencing. Baseline concentrations of

extracellular glutamate *in vivo* are in the nanomolar range[57] as glutamate transient decay is dependent on diffusion and uptake by membrane-bound transporters[58]. In the synaptic cleft of glutamatergic synapses, glutamate can reportedly reach as high as 1 mM[59,60], though this concentration has been contested[61], arguing the amount of transmitter released is highly variable and often nonsaturating[62,63]. Thus, it is not certain that this level of glutamate sensitivity will be detrimental to *in vivo* silencing applications. Punctate immunostaining patterns are suggestive of a synaptic localization for exogenously expressed GluCl receptors. Similar inhibitory receptors such as GlyR and $GABA_A$ are known to be clustered at synapses by binding of the anchor protein gephrin, which recognizes an 18-amino acid binding motif in the intracellular loop of the respective β subunit[64]. Sequence alignments indicate that neither GluCl α nor β subunits possess a gephrin binding motif, discounting the likelihood of clustering by this mechanism. Synaptic localization could be easily confirmed or denied by colocalization experiments with a postsynaptic density marker. If necessary, additional protein engineering strategies may be applied to the optimized GluCl tool to relieve synaptic receptor clustering.

Application of GluClv2.0

Since the initial proof-of concept study, the original GluCl/IVM tool has been used in conjunction with Channelrhodopsin-2-mediated activation to define an inhibitory microcircuit within the amygdala involved in mouse fear conditioning[65] and to identify a hypothalamic locus responsible for male mouse aggression and its close neuroanatomical

relationship to mating circuits[66]. An intersectional approach was used in former study to restrict GluCl expression to PKC-δ-containing GABAergic neurons of the central amygdala. This was achieved by transgenic expression GluCl α-CFP in all PKC-δ^+ neurons followed by stereotaxic injection of an AAV vector encoding GluCl β-YFP Y182F. While GluCl/IVM-induced silencing of PKC-δ^+ neurons yielded a statistically significant enhancement of conditional freezing, this behavioral result was confounded by a bimodal phenotype. Quantitative histological analysis again revealed considerable variation in expression of the virally injected β subunit among individual animals, reminiscent of the striatal proof-of-concept studies. Control animals transgenically expressing α alone or wild-type animals injected with β alone were not affected by treatment with 10 mg/kg IVM. While the present study confirms that α homomers are indeed trafficked to the plasma membrane, it raises the question of whether α homomer activation elicits sufficient chloride current to achieve neuronal silencing. For example, current responses recorded from GluCl α homomers expressed in *Xenopus* oocytes are 10-fold smaller than the αβ heteromeric responses[11,40]. A type of small slow-activating IVM-induced current has also been recorded from HEK293 cells which may result from α homomer expression, though this has not yet been confirmed (see Chapter 5, Figure 5.2). Additional *in vitro* neuronal silencing experiments should be conducted to compare the spike suppression capability of α homomers to αβ heteromers. Nevertheless, an intersectional approach is apparently still practical.

The optimized GluCl receptor, α-mXFP L9'F + β-mXFP Y182F RSR_AAA, dubbed 'GluCl version 2.0' or simply 'GluClv2.0', maintains the requirement for both α and β subunits. The new sequence modifications significantly improve receptor

sensitivity and subunit expression by preventing degradation of the β subunit and promoting its dimerization with the α subunit, in addition to relieving both subunits from the adverse effects of XFP oligomerization. The kinetic properties of the silencing tool have not been altered. An alternative orthogonal pharmacological silencing tool capable of activating and inactivating on shorter time scales has recently been constructed[67]. This tool employs chimeric nAChR-GlyR receptors of mammalian origins. The cognate synthetic nicotinic agonist has demonstrated weak to moderate binding of other endogenous nAChRs and the lack of co-assembly of chimeric subunits with endogenous nAChR subunits has not been verified. Even faster time-resolved neuronal silencing can be achieved using optogenetic techniques[68,69]. This method, however, is invasive and requires implantation of optical fibers that do not allow for manipulation of diffuse signaling networks. The duration of light-induced manipulation is also limited by heat generation which may alter neuronal activity or be damaging to cell health[70]. A separate attempt at improving IVM-induced silencing has also been made by modification of GlyR[71]. A single point mutation increased IVM sensitivity of GlyR by 100-fold, allowing activation in the nM range (i.e., similar to the original GluCl tool), while a separate point mutation eliminated glycine sensitivity. This modified GlyR tool has not been implemented *in vivo*. Future circuitry studies with this tool would be dependent on the assumption that endogenous GlyR expression is confined to spinal cord and brainstem neurons[72]. Experimental evidence, in fact, suggests a more widespread distribution of GlyR expression including higher brain regions such as the hippocampus, thalamus, amygdala, caudate-putamen and cerebral cortex[73-79]. Modified GlyRs would likely co-assemble with endogenous subunits yielding obscure results. GluCl receptors, on the

other hand, do not exist in mammalian neurons and GluClv2.0 manifests even greater sensitivity to IVM. We therefore believe the GluCl/IVM tool remains relevant and fills a niche for behavioral assays necessitating long-term neuronal inhibition (e.g., learning paradigms) and for assessing modulatory as opposed to regulatory roles in circuitry.

The aim of this project was to produce an optimized GluCl silencing tool via rational protein engineering strategies. Throughout this pursuit, a great deal has been learned about structure-function relationships and subunit expression patterns of GluCl. While the system is still not perfectly understood, the success of GluClv2.0 as an improved silencing tool has been demonstrated *in vitro*. The increased sensitivity and improved subunit expression of GluClv2.0 should allow lower doses of IVM to be administered for *in vivo* silencing, thereby alleviating concerns of off-target side effects and reducing the occurrence of suboptimal inhibition.

Materials and Methods

Site-Directed Mutagenesis

Codon optimized sequences of the *Caenorhabditis elegans* GluCl channel cloned into plasmid vector pcDNA3.1/V5-His TOPO (Invitrogen #K4800-01), including optGluCl αWT, optGluCl βWT, optGluCl α-XFP, and optGluCl β-XFP[12], were used in this study. Fluorescent protein insertions (XFP) include enhanced yellow (YFP) and cyan (CFP) variants and are located in the TM3-TM4 loop[11]. All constructs originate from the optimized codon sequences. For convenience, the 'opt' nomenclature has been omitted throughout most of this text. Point mutations were made using the QuikChange II XL site-directed mutagenesis kit (Agilent Technologies #200522) with PfuTurbo DNA polymerase (Agilent Technologies #600250). Forward and reverse primers for the (α)L9'F mutation are listed in Chapter 3. Mutant subunits in the current study were generated with the following forward and reverse primers (new codon is italicized in the forward primer): 5' – GGC GTG ACC ACC CTG *TTC* ACC ATG ACC ACC ATG – 3' and 5' – CAT GGT GGT CAT GGT GAA CAG GGT GGT CAC GCC – 3' for the (β)L9'F mutation; 5' – AC TTC GAC CTG GTG TCC *TTC* GCC CAC ACC – 3' and 5' – GGT GTG GGC GAA GGA CAC CAG GTC GAA GT – 3' for the (β)Y182F mutation; 5' – C AAC ACT GGC TCG *GCC* GGC TGC CTG CGC – 3' and 5' – GCG CAG GCA GCC GGC CGA GCC AGT GTT G – 3' for the (β)Y232A mutation; 5' – ACC AAC ACC GGC ATC *GCC* AGC TGC CTG AGG AC – 3' and 5' – GT CCT CAG GCA GCT GGC GAT GCC GGT GTT GGT – 3' for the (α)Y261A mutation; 5' – TAC CTG AGC TAC CAG TCC *AAG* CTG AGC AAA GAC CCC AAC – 3' and 5' –

GTT GGG GTC TTT GCT CAG CTT GGA CTG GTA GCT CAG GTA – 3' for the monomeric YFP A206K mutation; 5' – TG CGC CAG AAC GAC *GCC GCC GCC* GAG AAG GCG GCC C – 3' and 5' – G GGC CGC CTT CTC GGC GGC GGC GTC GTT CTG GCG CA – 3' for the (β)RSR_AAA mutation; 5' – CG GCC CGC AAG GCC CAG *GCA GCC GCC* GAG AAG CTG GAG ATG G –3' and 5'– C CAT CTC CAG CTT CTC GGC GGC TGC CTG GGC CTT GCG GGC CG – 3' for the (β)RRR_AAA mutation. The C-terminal tags V5 and 6-His are included in the plasmid vector and were added to the α and β subunits by point mutation of the stop codon with the following primers: 5' – G CAG AAC GTT CTG TTC *GGA* GCT AGC AAG GGC AA – 3' and 5' – TT GCC CTT GCT AGC TCC GAA CAG AAC GTT CTG C – 3' for the α subunit; 5' – CC GAG TCC CTG GTG *TTG* GCT AGC AAG G – 3' and 5' – C CTT GCT AGC CAA CAC CAG GGA CTC GG – 3' for the β subunit. All mutations were confirmed by DNA sequencing.

Cell culture

HEK293 cells were cultured, plated and transfected for electrophysiology and FlexStation assays as described in Chapter 3. For TIRF imaging experiments, HEK293 cells were plated on 35 mm glass bottom culture dishes (MatTEK #P35G-1.5-10-C) at 50,000 cells/dish and transfected following the same protocol used for the electrophysiology experiments described in Chapter 3. For Western blot analyses, HEK293 cells were plated in 10 cm dishes at 4×10^6 cells/dish and transfected with 16 μg DNA in 500 μl DMEM combined with 30 μl ExpressFect (Denville Scientific #E2650) in

500 µl DMEM that was preincubated for 20 minutes before adding to culture dishes containing 5 ml fresh culture medium. The transfection mix was removed after 4–6 hours and replaced with 10 ml of fresh culture medium. For all experiments, HEK293 cells were transfected 24 hours after plating and assayed 48 hours after transfection.

Hippocampal neurons were extracted from day 18 Wistar rat embryos[80] and plated at a density of 40,000 cells per dish on 35 mm glass bottom culture dishes coated with poly-DL-lysine (Sigma #P9011). Neurons were cultured in Neurobasal medium (Gibco #21103-049) containing 2% B27 (Gibco #17504-044), and 0.5 mM Glutamax (Gibco #35050). Medium was supplemented with 5% equine serum (Hyclone #SH30074) during plating. Cultures were maintained at 37°C and 5% CO_2 in a humidified incubator, with a 50% media exchange once per week. For imaging experiments, neurons were treated with 1 µM cytosine arabinoside (AraC; Sigma #C1768) on culture day 10 with a 100% media change the following day. Cultures used for electrophysiological experiments were not treated with AraC. Neurons were transiently transfected after 13-14 days in culture and assayed 24 hours later. Transfections were prepared per dish using 4 µg of plasmid DNA with 20 µg Nupherin-neuron (BIOMOL #SE-225) and 10 µl of Lipofectamine 2000 (Invitrogen #11668-019) diluted separately in 400 µl of Neurobasal without phenol red (Gibco #12348-017). Dilutions were individually incubated at room temperature for 15 minutes, then combined and incubated for another 45 minutes. An 800 µl volume of conditioned media was then removed from the neuronal culture dish and replaced with the 800 µl transfection mix. After incubating cultures for 1 hour at 37°C/5% CO_2, an 800 µl volume was removed from the dish and replaced with the original 800 µl of conditioned media.

Membrane Potential Measurements

Membrane Potential assays were performed on the FlexStation 3 multimode benchtop microplate reader using the BLUE formulation kit (Molecular Devices, #R8042) with the same dye preparation and data acquisition parameters described in Chapter 3. Glutamate and IVM drug preparation and dose-response data analysis is also described in Chapter 3.

Electrophysiology

Voltage-clamped HEK293 cells were recorded as described in Chapter 3. Neurons were whole-cell current-clamped using an Axopatch 200A amplifier with a CV201 headstage and Digidata 1200 series interface operated by Clampex 9.2 software (Axon Instruments). Spontaneous neuronal firing was recorded in Gap-free acquisition mode. Episodic Stimulation acquisition mode was used for executing stepwise current injections (-100 to 250 pA, 25 pA increments) to record evoked spike firing. Data was sampled at 50 kHz and lowpass filtered at 5 kHz. Neurons were perfused or incubated with artificial cerebrospinal fluid (ACSF) composed of (in mM): 110 NaCl, 5.4 KCl, 1.8 $CaCl_2$, 0.8 $MgCl_2$, 10 D-glucose, 10 HEPES, pH 7.4, 230 mOsm. Patch pipettes were made from borosilicate glass with resistances of 7–12 MΩ when filled with the following internal solution (in mM): 100 K-gluconate, 0.1 $CaCl_2$, 5 $MgCl_2$, 1.1 EGTA, 10 HEPES, 3 Mg-ATP, 0.3 GTP, 3 phosphocreatine, pH 7.2, 215 mOsm. IVM was dissolved in ACSF containing 0.1% DMSO and applied to cultures by bath perfusion or pre-incubation at 37°C/5% CO_2 for 15 minutes. All recordings were performed at ambient temperature.

Data was analyzed using Clampfit 9.2 software. Resting membrane potential was measured in the absence of any injected current and corrected for the liquid junction potential. Cells with a resting membrane potential of > −45 mV or with a seal resistance of < 100 MΩ or were omitted from analysis. The steady-state voltage response was plotted against the amount of current injected for a voltage-current (V-I) relationship. Input resistance of the cell was determined from the slope, according to Ohm's law, V = IR. Conductance was calculated as the inverse of resistance (G = 1/R = I/V). Induced spikes were counted manually and plotted against injected current.

Immunofluorescent labeling

Live, nonpermeabilized neurons were immunolabeled according to the protocol described in Glynn & McAllister, 2006[81]. A V5 epitope tag (GKPIPNPLLGLDST) followed by a 6-His tag (HHHHHH) already encoded in the pcDNA3.1 vector was added to the C-terminus of GluCl α and β subunits (including a 24-residue linker sequence, see Figure 4-19A) by mutation of the stop codon (see Site-Directed Mutagenesis). The 6-His tag was not utilized in these experiments. Surface receptors were labeled with primary mouse monoclonal anti-V5 antibody (1:200; Invitrogen #R960-25) followed by a conjugated secondary Alexa Fluor 555 donkey anti-mouse antibody (1:400; Invitrogen #A-31570). Antibodies were diluted into warm ACSF and applied sequentially, incubating each for 30 min at 37°C/5% CO_2 with appropriate wash steps. Live immunostained cultures were imaged immediately.

Western Blot Analysis

Whole-cell lysates were obtained from transiently transfected HEK293 cells using ice cold extraction buffer containing (in mM): 50 Tris, 50 NaCl, 1 EDTA, 1 EGTA, pH 7.4 and 1% NP40 supplemented with 1% protease inhibitor cocktail (Thermo Scientific #78410). The cell surface receptors were biotinylated and isolated for Western blot analysis using the Pierce Cell Surface Protein Isolation Kit (Thermo Scientific #89881). Cell samples (30 µl) were separated on 'Any kD' Mini-PROTEAN TGX Precast gels (Bio-Rad #456-9033) in Tris/Glycine/SDS running buffer (Bio-Rad #161-0732) at 200 V for 35 minutes. Gel bands were transferred onto presoaked Protran nitrocellulose membranes (Whatman #10485376) in buffer containing 20% methanol and 10% Tris-glycine SDS at 15 V for 20 minutes. Nitrocellulose membranes were initially blocked in 10% milk in TBST (TBS + 0.1% Tween-20; Bio-Rad #170-6435, Sigma #P1379) and then incubated with rabbit anti-GFP antibody (1:1000; Invitrogen #A11122) in 5% BSA in TBST with 10% NaN_3 overnight to probe for GluCl β-mYFP subunit expression. Protein bands were detected by enhanced chemiluminescence (Western Lightning Plus-ECL; PerkinElmer #NEL103001EA) using goat anti-rabbit horseradish peroxidase (1:5000; Promega #W4011) in 5% BSA in TBST and developed on film (Amersham Hyperfilm ECL). The ~72 kDa molecular weight band was identified using the SeeBlue Plus2 prestained protein standard (Invitrogen #LC5925). ImageJ software (National Institutes of Health; http://rsb.info.nih.gov/ij/) was used for quantification of band intensity.

Imaging

All cultured neurons and HEK293 cells and were imaged live at 37°C in a stage-mounted culture dish incubator (Warner Instruments). Transiently transfected HEK293 cells were imaged by Total Internal Reflection Fluorescence (TIRF) microscopy, which enabled visualization of fluorescent receptors expressed in the plasma membrane and nearby intracellular vesicles within 200 nm of the cell-coverslip interface. Prior to imaging, cell culture medium was replaced with phenol red-free CO_2-independent Leibovitz L-15 medium (Gibco #21083-027). TIRF images were obtained using an inverted microscope (Olympus IX81) with a 100x/1.45 NA Plan Apochromat oil objective. A T-cube stepper motor (Thorlabs) was used to control the position of the fiber optic and TIRF evanescent field illumination. A 488 nm laser was used to excite monomeric YFP fluorescence. Images were acquired with MetaMorph Premier software (Molecular Devices) at 16-bit resolution over 512×512 pixels and captured using a back-illuminated EMCCD camera (iXON DU-897) supported by ANDOR iQ2 software (Andor Technology).

Transiently transfected hippocampal neuron cultures were imaged using a laser-scanning confocal microscope (Nikon Eclipse C1si) with a 63x/1.4 NA VC Plan Apochromat oil objective. Monomeric YFP fluorescence was acquired with 514 nm laser excitation. Alexa 555 and pDsRED2 (Clontech #632409) fluorescence was acquired with 561 nm laser excitation. Images were collected as z-stacks at a step size of 1.0 μm with 16-bit resolution over 512×512 pixels and a dwell time of 6.72 μs.

For confocal image analysis, the two different fluorescent signal intensities were correlated on a pixel-by-pixel basis using the Colocalization Colormap ImageJ plug-in

(Adam Gorlewicz, http://sites.google.com/site/colocalizationcolormap/home) based on the algorithm by Jaskolski et al., 2005[82]. The correlation of a pair of pixels was calculated as follows:

$$nMDP_{x,y} = \frac{(Ia - \overline{Ia})(Ib - \overline{Ib})}{(Ia_{max} - \overline{Ia})(Ib_{max} - \overline{Ib})}$$

Ia	intensity for the given pixel in image a
$\overline{Ia}$	average intensity of image a
Ia_{max}	the highest pixel intensity in image a
Ib	intensity for the given pixel in image b
$\overline{Ib}$	average intensity of image b
Ib_{max}	the highest pixel intensity in image b

The normalized mean deviation product (nMDP) values for each pixel range from −1 to 1 and can be visualized on a color scale. Values < 0 are represented by cold colors for exclusion and values > 0 are shown in hot colors for colocalization. Zero values indicate black background. For the experimental conditions of the current study, the average of all positive (colocalized) nMDP values corresponds to total receptor surface expression, while the average number of perfectly correlated pixels (i.e., where nMDP = 1) indicates the relative amounts of each receptor subunit.

Statistics

Pooled data are shown as means ± SEM. Boxplots represent the mean, median, 25^{th}, and 75^{th} percentiles. Statistical significance ($P < 0.05$) was determined by one-way analysis of variance (ANOVA) on ranks using multiple pairwise comparison.

Acknowledgements

Thanks to Sheri McKinney for providing hippocampal neuron cultures.

References

1. Lerchner W, Xiao C, Nashmi R, Slimko EM, van Trigt L, Lester HA, Anderson DJ. (2007) Reversible silencing of neuronal excitability in behaving mice by a genetically targeted, ivermectin-gated Cl- channel. *Neuron* **54**:35–49.

2. Anden NE, Hfuxe K, Hamberger B, Hokfelt T. (1966) A quantitative study on the nigro-neostriatal dopamine neuron system in the rat. *Acta Physiol Scand* **67**:306–312.

3. Schwarcz R, Fuxe K, Agnati LF, Hokfelt T, Coyle JT. (1979) Rotational behaviour in rats with unilateral striatal kainic acid lesions: a behavioural model for studies on intact dopamine receptors. *Brain Res* **170**:485–495.

4. Burdett EC, Heckmann RA, Ochoa R. (1997) Evaluation of five treatment regimens and five diagnostic methods for murine mites (Myocoptes musculinus and Myobia musculi). *Contemp Top Lab Anim Sci* **36**:73–76.

5. Schinkel AH, Smit JJ, van Tellingen O, Beijnen JH, Wagenaar E, van Deemter L, Mol CA, van der Valk MA, Robanus-Maandag EC, te Riele HP, et al. (1994) Disruption of the mouse mdr1a P-glycoprotein gene leads to a deficiency in the blood-brain barrier and to increased sensitivity to drugs. *Cell* **77**:491–502.

6. Roder JD, Stair EL. (1998) An overview of ivermectin toxicosis. *Vet Hum Toxicol* **40**:369–370.

7. Adelsberger H, Lepier A, Dudel J. (2000) Activation of rat recombinant α(1)β(2)γ(2S) GABA(A) receptor by the insecticide ivermectin. *Eur J Pharmacol* **394**:163–170.

8. Khakh BS, Proctor WR, Dunwiddie TV, Labarca C, Lester HA. (1999) Allosteric control of gating and kinetics at P2X(4) receptor channels. *J Neurosci* **19**:7289–7299.

9. Krause RM, Buisson B, Bertrand S, Corringer PJ, Galzi JL, Changeux JP, Bertrand D. (1998) Ivermectin: a positive allosteric effector of the α7 neuronal nicotinic acetylcholine receptor. *Mol Pharmacol* **53**:283–294.

10. Shan Q, Haddrill JL, Lynch JW. (2001) Ivermectin, an unconventional agonist of the glycine receptor chloride channel. *J Biol Chem* **276**:12556–12564.

11. Li P, Slimko EM, Lester HA. (2002) Selective elimination of glutamate activation and introduction of fluorescent proteins into a Caenorhabditis elegans chloride channel. *FEBS Lett* **528**:77–82.

12. Slimko EM, Lester HA. (2003) Codon optimization of Caenorhabditis elegans GluCl ion channel genes for mammalian cells dramatically improves expression levels. *J Neurosci Methods* **124**:75–81.

13. Slimko EM, McKinney S, Anderson DJ, Davidson N, Lester HA. (2002) Selective electrical silencing of mammalian neurons in vitro by the use of invertebrate ligand-gated chloride channels. *J Neurosci* **22**:7373–7379.

14. Ellgaard L, Helenius A. (2003) Quality control in the endoplasmic reticulum. *Nat Rev Mol Cell Biol* **4**:181–191.

15. Teasdale RD, Jackson MR. (1996) Signal-mediated sorting of membrane proteins between the endoplasmic reticulum and the golgi apparatus. *Annu Rev Cell Dev Biol* **12**:27–54.

16. Hurtley SM, Helenius A. (1989) Protein oligomerization in the endoplasmic reticulum. *Annu Rev Cell Biol* **5**:277–307.

17. Klausner RD, Sitia R. (1990) Protein degradation in the endoplasmic reticulum. *Cell* **62**:611–614.

18. Nishimura N, Balch WE. (1997) A di-acidic signal required for selective export from the endoplasmic reticulum. *Science* **277**:556–558.

19. Nishimura N, Bannykh S, Slabough S, Matteson J, Altschuler Y, Hahn K, Balch WE. (1999) A di-acidic (DXE) code directs concentration of cargo during export from the endoplasmic reticulum. *J Biol Chem* **274**:15937–15946.

20. Mossessova E, Bickford LC, Goldberg J. (2003) SNARE selectivity of the COPII coat. *Cell* **114**:483–495.

21. Mancias JD, Goldberg J. (2008) Structural basis of cargo membrane protein discrimination by the human COPII coat machinery. *EMBO J* **27**:2918–2928.

22. Jackson MR, Nilsson T, Peterson PA. (1990) Identification of a consensus motif for retention of transmembrane proteins in the endoplasmic reticulum. *EMBO J* **9**:3153–3162.

23. Munro S, Pelham HR. (1987) A C-terminal signal prevents secretion of luminal ER proteins. *Cell* **48**:899–907.

24. Zerangue N, Schwappach B, Jan YN, Jan LY. (1999) A new ER trafficking signal regulates the subunit stoichiometry of plasma membrane K(ATP) channels. *Neuron* **22**:537–548.

25. Margeta-Mitrovic M, Jan YN, Jan LY. (2000) A trafficking checkpoint controls GABA(B) receptor heterodimerization. *Neuron* **27**:97–106.

26. Bichet D, Cornet V, Geib S, Carlier E, Volsen S, Hoshi T, Mori Y, De Waard M. (2000) The I-II loop of the Ca2+ channel α1 subunit contains an endoplasmic reticulum retention signal antagonized by the β subunit. *Neuron* **25**:177–190.

27. Scott DB, Blanpied TA, Swanson GT, Zhang C, Ehlers MD. (2001) An NMDA receptor ER retention signal regulated by phosphorylation and alternative splicing. *J Neurosci* **21**:3063–3072.

28. Standley S, Roche KW, McCallum J, Sans N, Wenthold RJ. (2000) PDZ domain suppression of an ER retention signal in NMDA receptor NR1 splice variants. *Neuron* **28**:887–898.

29. Xia H, Hornby ZD, Malenka RC. (2001) An ER retention signal explains differences in surface expression of NMDA and AMPA receptor subunits. *Neuropharmacology* **41**:714–723.

30. Boyd GW, Doward AI, Kirkness EF, Millar NS, Connolly CN. (2003) Cell surface expression of 5-hydroxytryptamine type 3 receptors is controlled by an endoplasmic reticulum retention signal. *J Biol Chem* **278**:27681–27687.

31. Sadtler S, Laube B, Lashub A, Nicke A, Betz H, Schmalzing G. (2003) A basic cluster determines topology of the cytoplasmic M3-M4 loop of the glycine receptor α1 subunit. *J Biol Chem* **278**:16782–16790.

32. Srinivasan R, Pantoja R, Moss FJ, Mackey ED, Son CD, Miwa J, Lester HA. (2011) Nicotine up-regulates α4β2 nicotinic receptors and ER exit sites via stoichiometry-dependent chaperoning. *J Gen Physiol* **137**:59–79.

33. Brock C, Boudier L, Maurel D, Blahos J, Pin JP. (2005) Assembly-dependent surface targeting of the heterodimeric GABAB Receptor is controlled by COPI but not 14-3-3. *Mol Biol Cell* **16**:5572–5578.

34. Michelsen K, Yuan H, Schwappach B. (2005) Hide and run. Arginine-based endoplasmic-reticulum-sorting motifs in the assembly of heteromultimeric membrane proteins. *EMBO Rep* **6**:717–722.

35. Yuan H, Michelsen K, Schwappach B. (2003) 14-3-3 dimers probe the assembly status of multimeric membrane proteins. *Curr Biol* **13**:638–646.

36. Hibbs RE, Gouaux E. (2011) Principles of activation and permeation in an anion-selective Cys-loop receptor. *Nature* **474**:54–60.

37. Yang F, Moss LG, Phillips GN, Jr. (1996) The molecular structure of green fluorescent protein. *Nat Biotechnol* **14**:1246–1251.

38. Zacharias DA, Violin JD, Newton AC, Tsien RY. (2002) Partitioning of lipid-modified monomeric GFPs into membrane microdomains of live cells. *Science* **296**:913–916.

39. Zacharias DA. (2002) Sticky caveats in an otherwise glowing report: oligomerizing fluorescent proteins and their use in cell biology. *Sci STKE* **2002**:pe23.

40. Cully DF, Vassilatis DK, Liu KK, Paress PS, Van der Ploeg LH, Schaeffer JM, Arena JP. (1994) Cloning of an avermectin-sensitive glutamate-gated chloride channel from Caenorhabditis elegans. *Nature* **371**:707–711.

41. Forrester SG, Beech RN, Prichard RK. (2004) Agonist enhacement of macrocyclic lactone activity at a glutamate-gated chloride channel subunit from Haemonchus contortus. *Biochem Pharmacol* **67**:1019–1024.

42. Forrester SG, Prichard RK, Beech RN. (2002) A glutamate-gated chloride channel subunit from Haemonchus contortus: expression in a mammalian cell line, ligand binding, and modulation of anthelmintic binding by glutamate. *Biochem Pharmacol* **63**:1061–1068.

43. Bonifacino JS, Cosson P, Shah N, Klausner RD. (1991) Role of potentially charged transmembrane residues in targeting proteins for retention and degradation within the endoplasmic reticulum. *EMBO J* **10**:2783–2793.

44. Bonifacino JS, Lippincott-Schwartz J. (1991) Degradation of proteins within the endoplasmic reticulum. *Curr Opin Cell Biol* **3**:592–600.

45. Gorrie GH, Vallis Y, Stephenson A, Whitfield J, Browning B, Smart TG, Moss SJ. (1997) Assembly of GABAA receptors composed of α1 and β2 subunits in both cultured neurons and fibroblasts. *J Neurosci* **17**:6587–6596.

46. Merlie JP, Lindstrom J. (1983) Assembly in vivo of mouse muscle acetylcholine receptor: identification of an α subunit species that may be an assembly intermediate. *Cell* **34**:747–757.

47. Blount P, Merlie JP. (1990) Mutational analysis of muscle nicotinic acetylcholine receptor subunit assembly. *J Cell Biol* **111**:2613–2622.

48. Green WN. (1999) Ion channel assembly: creating structures that function. *J Gen Physiol* **113**:163–170.

49. Moroni M, Bermudez I. (2006) Stoichiometry and pharmacology of two human α4β2 nicotinic receptor types. *J Mol Neurosci* **30**:95–96.

50. Nelson ME, Kuryatov A, Choi CH, Zhou Y, Lindstrom J. (2003) Alternate stoichiometries of α4β2 nicotinic acetylcholine receptors. *Mol Pharmacol* **63**:332–341.

51. Zhou Y, Nelson ME, Kuryatov A, Choi C, Cooper J, Lindstrom J. (2003) Human α4β2 acetylcholine receptors formed from linked subunits. *J Neurosci* **23**:9004–9015.

52. Bormann J, Rundstrom N, Betz H, Langosch D. (1993) Residues within transmembrane segment M2 determine chloride conductance of glycine receptor homo- and hetero-oligomers. *EMBO J* **12**:3729–3737.

53. Becker CM, Hoch W, Betz H. (1988) Glycine receptor heterogeneity in rat spinal cord during postnatal development. *EMBO J* **7**:3717–3726.

54. Langosch D, Thomas L, Betz H. (1988) Conserved quaternary structure of ligand-gated ion channels: the postsynaptic glycine receptor is a pentamer. *Proc Natl Acad Sci U S A* **85**:7394–7398.

55. Grudzinska J, Schemm R, Haeger S, Nicke A, Schmalzing G, Betz H, Laube B. (2005) The beta subunit determines the ligand binding properties of synaptic glycine receptors. *Neuron* **45**:727–739.

56. Gleitsman KR, Shanata JA, Frazier SJ, Lester HA, Dougherty DA. (2009) Long-range coupling in an allosteric receptor revealed by mutant cycle analysis. *Biophys J* **96**:3168–3178.

57. Herman MA, Jahr CE. (2007) Extracellular glutamate concentration in hippocampal slice. *J Neurosci* **27**:9736–9741.

58. Diamond JS, Jahr CE. (1997) Transporters buffer synaptically released glutamate on a submillisecond time scale. *J Neurosci* **17**:4672–4687.

59. Clements JD. (1996) Transmitter timecourse in the synaptic cleft: its role in central synaptic function. *Trends Neurosci* **19**:163–171.

60. Clements JD, Lester RA, Tong G, Jahr CE, Westbrook GL. (1992) The time course of glutamate in the synaptic cleft. *Science* **258**:1498–1501.

61. Bergles DE, Diamond JS, Jahr CE. (1999) Clearance of glutamate inside the synapse and beyond. *Curr Opin Neurobiol* **9**:293–298.

62. Frerking M, Wilson M. (1996) Saturation of postsynaptic receptors at central synapses? *Curr Opin Neurobiol* **6**:395–403.

63. McAllister AK, Stevens CF. (2000) Nonsaturation of AMPA and NMDA receptors at hippocampal synapses. *Proc Natl Acad Sci U S A* **97**:6173–6178.

64. Meyer G, Kirsch J, Betz H, Langosch D. (1995) Identification of a gephyrin binding motif on the glycine receptor beta subunit. *Neuron* **15**:563–572.

65. Haubensak W, Kunwar PS, Cai H, Ciocchi S, Wall NR, Ponnusamy R, Biag J, Dong HW, Deisseroth K, Callaway EM, Fanselow MS, Luthi A, Anderson DJ. (2010) Genetic dissection of an amygdala microcircuit that gates conditioned fear. *Nature* **468**:270–276.

66. Lin D, Boyle MP, Dollar P, Lee H, Lein ES, Perona P, Anderson DJ. (2011) Functional identification of an aggression locus in the mouse hypothalamus. *Nature* **470**:221–226.

67. Magnus CJ, Lee PH, Atasoy D, Su HH, Looger LL, Sternson SM. (2011) Chemical and genetic engineering of selective ion channel-ligand interactions. *Science* **333**:1292–1296.

68. Gradinaru V, Thompson KR, Deisseroth K. (2008) eNpHR: a Natronomonas halorhodopsin enhanced for optogenetic applications. *Brain Cell Biol* **36**:129–139.

69. Zhang F, Wang LP, Brauner M, Liewald JF, Kay K, Watzke N, Wood PG, Bamberg E, Nagel G, Gottschalk A, Deisseroth K. (2007) Multimodal fast optical interrogation of neural circuitry. *Nature* **446**:633–639.

70. Tye KM, Deisseroth K. (2012) Optogenetic investigation of neural circuits underlying brain disease in animal models. *Nat Rev Neurosci* **13**:251–266.

71. Lynagh T, Lynch JW. (2010) An improved ivermectin-activated chloride channel receptor for inhibiting electrical activity in defined neuronal populations. *J Biol Chem* **285**:14890–14897.

72. Rajendra S, Lynch JW, Schofield PR. (1997) The glycine receptor. *Pharmacol Ther* **73**:121–146.

73. Betz H. (1991) Glycine receptors: heterogeneous and widespread in the mammalian brain. *Trends Neurosci* **14**:458–461.

74. Danober L, Pape HC. (1998) Strychnine-sensitive glycine responses in neurons of the lateral amygdala: an electrophysiological and immunocytochemical characterization. *Neuroscience* **85**:427–441.

75. Darstein M, Landwehrmeyer GB, Kling C, Becker CM, Feuerstein TJ. (2000) Strychnine-sensitive glycine receptors in rat caudatoputamen are expressed by cholinergic interneurons. *Neuroscience* **96**:33–39.

76. Malosio ML, Marqueze-Pouey B, Kuhse J, Betz H. (1991) Widespread expression of glycine receptor subunit mRNAs in the adult and developing rat brain. *EMBO J* **10**:2401–2409.

77. McCool BA, Farroni JS. (2001) Subunit composition of strychnine-sensitive glycine receptors expressed by adult rat basolateral amygdala neurons. *Eur J Neurosci* **14**:1082–1090.

78. Naas E, Zilles K, Gnahn H, Betz H, Becker CM, Schroder H. (1991) Glycine receptor immunoreactivity in rat and human cerebral cortex. *Brain Res* **561**:139–146.

79. Rampon C, Luppi PH, Fort P, Peyron C, Jouvet M. (1996) Distribution of glycine-immunoreactive cell bodies and fibers in the rat brain. *Neuroscience* **75**:737–755.

80. Li YX, Zhang Y, Lester HA, Schuman EM, Davidson N. (1998) Enhancement of neurotransmitter release induced by brain-derived neurotrophic factor in cultured hippocampal neurons. *J Neurosci* **18**:10231–10240.

81. Glynn MW, McAllister AK. (2006) Immunocytochemistry and quantification of protein colocalization in cultured neurons. *Nat Protoc* **1**:1287–1296.

82. Jaskolski F, Mulle C, Manzoni OJ. (2005) An automated method to quantify and visualize colocalized fluorescent signals. *J Neurosci Methods* **146**:42–49.